Università degli Studi di Padova

Dipartimento di Biologia

CORSO DI DOTTORATO DI RICERCA IN BIOSCIENZE E BIOTECNOLOGIE

CURRICOLO NEUROBIOLOGIA

CICLO XXIX

THE MITOCHONDRIA FISSION PROTEIN DRP1 IS REQUIRED FOR MUSCLE MASS MAINTENANCE

Tesi redatta con il contributo finanziario di Fondazione per la Ricerca Biomedica Avanzata

Coordinatore: Ch.mo Prof. Paolo Bernardi

Supervisore: Ch.mo Prof. Marco Sandri

Dottorando: Giulia Favaro

INDEX

ABBREVIATIONS

ATG: autophagy related gene

ATP: adenosine triphosphate

BMP: bone morphogenetic protein

CMT2A: Charcot-Marie-Tooth type 2A

CSA: cross-sectional area

DOA: dominant optic atrophy

Drp1: Dynamin related protein 1

EB: experimental buffer

ER: endoplasmic reticulum

FCCP: carbonyl cyanide-p-trifluoromethoxyphenylhydrazone

FDB: flexor digitorum brevis

GED: guanosine triphosphatase effector domain

GH: growth hormone

GSK3β: glycogen synthase kinase 3 beta

GTPase: guanosine triphosphatase

HSA: human skeletal actin

IGF-1: insulin-like growth factor

IMF: intermyofibrillar

IMM: inner mitochondrial membrane

KO: knock-out

MCU: mitochondrial calcium uniporter

Mff: mitochondrial fissiom factor

Mfn1: mitofusin1

Mfn2: mitofusin2

MiD: mitochondrial division

MLC1f: myosin heavy chain 1 fast

mTOR: mammalian target of rapamycin

mt-Keima: Mitochondria-targeted mKeima

MyHC: myosin heavy chain

OMM: outer mitochondrial membrane

Opa1: optic atrophy 1

PTP: permeability transition pore

RCC: respiratory chain complexes

RCR: respiratory control ratio

RCS: respiratory chain supercomplexes

ROS: reactive oxygen species

RyR: ryanodine receptor

SDH: succinate dehydrogenase

SERCA: sarco/endoplasmic reticulum Ca^{2+} ATPase

SR: sarcoplasmic reticulum

SS: subsarcolemmal

TMRM: tetramethylrhodamine

T-tubules: transverse tubules

UPR: unfolded protein response

UPS: ubiquitin proteasome system

WT: wildtype

4EBP1: 4 E binding protein 1

SUMMARY

The skeletal muscle accounts for almost 40% of total body mass and represents a major site of metabolic activity. Skeletal muscle is a dynamic tissue: exercise and hormonal stimulation lead to an increase in protein synthesis and fiber size, a process called hypertrophy. Conversely, the loss of muscle mass, named atrophy, is the result of an increase in protein degradation. Muscle atrophy can occur in several pathological conditions like cancer, diabetes, chronic heart failure, AIDS, and during aging.

Mitochondria play a key role in muscle homeostasis, because they provide its high energy demand. Indeed, atrophying conditions are characterized by alterations of the mitochondrial network (Romanello et al., 2010). So, the maintenance of a functional mitochondrial population is important for tissues that are highly structured and metabolically active such as neurons, cardiac and skeletal muscle. In these tissues, mitochondria quality control depends only on mitochondria shaping machinery which include fusion and fission processes. Mitochondrial fusion leads to the formation of an interconnected network, facilitating the redistribution of metabolites, proteins and mtDNA. On the contrary, fission generates isolated and fragmented mitochondria allowing the specific removal of dysfunctional and damaged organelles via mitophagy. The importance of mitochondria fusion and fission in skeletal muscles was underlined by transcriptomic and proteomic analysis showing the progressive loss during ageing of mitochondrial proteins involved in these mechanisms (Ibedunjo et al., 2013).

The key player of mitochondria fission is Dynamin Related protein-1, Drp1, a cytosolic guanosine triphosphatase (GTPase) that is recruited to the outer mitochondria membrane (OMM) of damaged mitochondria, where it assembles into multimeric ring complexes inducing mitochondria fragmentation (Smirnova et al., 2001). Recent findings indicate that muscle-specific Drp1 overexpression triggers muscle mass loss and decreases exercise performance (Touvier et al., 2015), confirming previous data demonstrating that overexpression of the fission

machinery in skeletal muscle is sufficient to induce mitochondrial dysfunction and muscle atrophy (Romanello et al., 2010). Since overexpression studies are often confounded by off target effects, we decided to use a loss of function approach to study the role of Drp1 in skeletal muscle mass maintenance. Therefore, we generated a muscle-specific Drp1 knock-out mouse model (MLC1f-Drp1 KO). The conditional deletion of Drp1 resulted in a lethal phenotype and an important muscle atrophy. Muscle mass loss is mediated by a decrease in protein synthesis mainly due to the activation of Unfolded Protein Response (UPR) pathway that blocks general translation through eif2α phosphorylation. UPR led also to the up-regulation in skeletal muscle of the cytokine FGF21. The observed FGF21 induction resulted in metabolic changes such as hypoglycemia, growth hormone (GH) resistance and decreased insulin-like growth factor IGF-1 expression in the liver, and a consequent reduced animal size. In addition, Drp1 ablation triggered protein degradation through the induction of FoxO3, a major regulator of protein breakdown. In particular, FoxO3 is the responsible of the increased expression of Atrogin1 and MuRF1, two muscle-specific E3 ubiquitin-ligases, and MUSA1, a novel ubiquitin-ligase, meaning that the Ubiquitin-Proteasome system is activated in knock-out animals. Moreover, real-time PCR analyses revealed the induction of several genes implicated in different step of the autophagic flux, suggesting that also Autophagy-Lysosome system contributes to protein degradation in MLC1f-Drp1 knock-out.

Considering the severity of the phenotype, we decided to investigate the role of Drp1 in adult muscles through the generation of muscle-specific inducible Drp1 knock-out mice (HSA-Drp1 KO). We surprisingly found that Drp1 deletion in adulthood resulted in body weight loss secondary to muscle atrophy. Moreover, knock-out mice appeared weaker compared to controls. Indeed, both absolute and normalized force were affected in Drp1-deleted animals, suggesting that muscle weakness was not dependent on muscle atrophy. In addition, the absence of mitochondria division impaired mitochondria size and morphology leading to the presence of enlarged mitochondria with a reduced functionality. In fact,

mitochondria membrane potential and respiration efficiency were affected in HSA-Drp1 KO muscles.

In order to explain the mechanism involved in muscle atrophy, we found that the activation of UPR pathway, and of degradative systems involved in protein breakdown are conserved between conditional and inducible models. However, *in vivo* protein synthesis rate is not affected during adulthood.

Muscle weakness, UPR activation and mitochondria dysfunction can be triggered by an impairment in calcium physiology. We analyzed calcium homeostasis in flexor digitorum brevis (FDB)-isolated fibers and found that the deletion of Drp1 impaired sarcoplasmic reticulum (SR)-calcium release, which is prevented by the inhibition of mitochondrial calcium uptake through mitochondrial calcium uniporter (MCU) silencing. Importantly, these alterations precede muscle mass loss, suggesting that dysregulation of calcium homeostasis can be the cause of the severe phenotype. These findings indicate that mitochondrial dynamics and mophology are important for the maintenance of the physiology of calcium signaling at least in skeletal muscle.

Finally, knock-out mice analyzed after 7 months from Drp1 deletion showed signs of precocious aging and a severe muscle mass loss. Moreover, the chronic Drp1 ablation led to myofibers degeneration and regeneration, as shown by the accumulation of centrally nucleated fibers. All together, our results, strongly support the involvement of mitochondrial morphology and/or function in the activation of signaling pathways that control muscle mass. Thus, therapeutic interventions that maintain a fine equilibrium of mitochondrial fusion/fission processes in needed to preserve muscle mass and prevent muscle wasting.

RIASSUNTO

I muscoli scheletrici costituiscono il 40% di tutto l'organismo e sono caratterizzati da un'elevata attività metabolica. Il muscolo scheletrico è un tessuto molto plastico e dinamico che adatta la propria massa in risposta a diversi stimoli. L'esercizio fisico e gli stimoli anabolici, per esempio, inducono un aumento della sintesi proteica e della massa muscolare, un processo chiamato ipertrofia. Un aumento della degradazione proteica, invece, provoca perdita della massa muscolare, detta atrofia. L'atrofia muscolare è una conseguenza di diverse condizioni patologiche come cancro, diabete, AIDS, cardiomiopatie ed invecchiamento.

I mitocondri hanno un ruolo chiave nel mantenimento dell'omeostasi muscolare in quanto forniscono l'energia necessaria al muscolo. Infatti, l'atrofia muscolare è caratterizzata da alterazioni nel *network* mitocondriale (Romanello et al., 2010). Per questo motivo, è particolarmente importante preservare la funzionalità mitocondriale nei tessuti caratterizzati da un'elevata attività metabolica come neuroni, muscoli scheletrico e cardiaco. In questi tessuti, il controllo della funzionalità dei mitocondri è esclusivamente basato sui processi di fusione e fissione mitocondriale. La fusione mitocondriale aumenta la connessione tra i mitocondri in modo da favorire lo scambio di proteine, metaboliti e DNA mitocondriale. La fissione, invece, porta alla frammentazione di questi organelli permettendo, così, la rimozione dei mitocondri disfunzionanti attraverso un meccanismo chiamato mitofagia. L'importanza di questi due processi nel muscolo scheletrico è stata recentemente evidenziata da analisi di trascrittomica e di proteomica, i quali hanno dimostrato la progressiva perdita, durante l'invecchiamento, di proteine mitocondriali coinvolte nei meccanismi di fusione e fissione (Ibedunjo et al., 2013).

Drp1, una proteina appartenente alla famiglia delle GTPasi, ha un ruolo chiave nella fissione mitocondriale. In particolare, Drp1 è una proteina citosolica che trasloca sulla membrana mitocondriale esterna dei mitocondri danneggiati e disfunzionanti, dove si assembla formando un anello multimerico che induce la divisione

mitocondriale (Smirnova et al., 2001). Recentemente alcuni studi hanno dimostrato che l'overespressione di Drp1 nel muscolo induce perdita della massa muscolare e riduce la performance durante l'esercizio fisico (Touvier et al., 2015). Ciò conferma alcuni dati ottenuti precedentemente, i quali dimostrano che l'aumentata espressione nel muscolo scheletrico di altre proteine coinvolte nella fissione mitocondriale, inducono atrofia muscolare ed una diminuita funzionalità dei mitocondri (Romanello et al., 2010). Purtroppo, gli studi basati sulla tecnica dell'overespressione di proteine sono spesso accompagnati da effetti secondari, perciò abbiamo deciso di studiare il ruolo di Drp1 nel muscolo scheletrico utilizzando un approcio di tipo *loss of function*. Abbiamo, quindi, generato un modello di topo Drp1 *knock-out* muscolo-specifico (MLC1f-Drp1 KO). La delezione di Drp1 nel muscolo è risultata essere letale e causa atrofia muscolare. La perdita della massa muscolare è mediata da una riduzione della sintesi proteica, che è dovuta all'attivazione della via di segnale UPR. La via UPR, infatti, blocca la sintesi proteica attraverso la fosforilazione del fattore eif2α. Inoltre, la via UPR induce un aumento dei livelli di espressione della citochina FGF21 nel muscolo scheletrico. L'induzione di FGF21 determina alcuni importanti cambiamenti nel metabolismo degli animali *knock-out*: ipoglicemia, resistenza all'ormone della crescita e diminuzione dell'espressione di IGF-1 nel fegato. Questi cambiamenti sono responsabili del fatto che gli animali Drp1-deleti appaiono più piccoli rispetto ai controlli. La mancata espressione di Drp1 nel muscolo induce anche un aumento nella degradazione delle proteine attraverso FoxO3. FoxO3 è un fattore che controlla le vie degradative nel muscolo scheletrico. In particolare, FoxO3 induce l'espressione di Atrogin1 e MuRF1, due ubiquitine ligasi muscolo-specifiche, e di MUSA1, un'ubiquitina ligasi recentemente identificata nel nostro laboratorio (Sartori et al., 2013). Questi dati dimostrano l'attivazione del sistema ubiquitina-proteasoma nei muscoli degli animali *knock-out*. Inoltre, l'analisi attraverso real-time PCR di alcuni geni coinvolti in diversi step del flusso autofagico, suggerisce che anche l'attivazione del sistema autofagia-lisosoma contribuisce alla degradazione proteica nel nostro modello animale.

Considerando che la delezione di Drp1 induce la morte precoce dell'animale, abbiamo deciso di studiare il suo ruolo nel muscolo adulto attraverso la generazione di un modello *knock-out* inducibile muscolo-specifico (HSA-Drp1 KO). Sorprendentemente, la delezione di Drp1 in età adulta provoca una significativa perdita di peso corporeo a causa della riduzione della massa muscolare. Inoltre, i topi *knock-out* appaiono più deboli in quanto sia la forza assoluta, sia la forza normalizzata, sono più basse rispetto ai controlli. Ciò suggerisce che la diminuzione della forza è indipendente dall'atrofia.

L'assenza della divisione mitocondriale impatta anche sulla dimensione e sulla morfologia dei mitocondri, portando all'accumulo di mitocondri più grandi, ma con una diminuita funzionalità. Infatti, i mitocondri nei muscoli *knock-out* sono caratterizzati da alterazioni nel mantenimento del potenziale di membrana e una ridotta efficienza respiratoria.

Studiando i meccanismi coinvolti nell'atrofia muscolare, abbiamo notato che la via di segnale UPR e i sistemi di degradazione (Ubiquitina-Proteasoma e Autofagia-Lisosoma) sono conservati nei due modelli animali. Tuttavia, la sintesi proteica non risulta alterata in età adulta.

La ridotta forza muscolare, l'attivazione della via UPR e la disfunzione mitocondriale possono essere dovute ad una alterazione della fisiologia del calcio. Per questo motivo, abbiamo analizzato l'omeostasi del calcio nelle fibre muscolari derivate dal muscolo FDB. I risultati dimostrano che la delezione di Drp1 altera il rilascio di calcio dal reticolo sarcoplasmatico. Ciò si può prevenire inibendo l'ingresso di calcio nei mitocondri, attraverso il silenziamento di MCU. È interessante notare che queste alterazioni precedono la perdita della massa muscolare, suggerendo che esse possano essere la causa del fenotipo osservato. Questi risultati indicano che la dinamica e la morfologia mitocondriali potrebbero influenzare in parte il controllo dei livelli di calcio nel muscolo scheletrico.

Infine, gli animali *knock-out*, analizzati 7 mesi dopo la delezione di Drp1, mostrano segni di invecchiamento precoce e una grave atrofia muscolare. Inoltre, i muscoli sono caratterizzati da degenerazione e rigenerazione delle fibre muscolari, come

evidenzia l'accumulo di fibre centro-nucleate. Riassumendo, i nostri risultati dimostrano che la morfologia e la funzione dei mitocondri influenzano l'attivazione di vie di segnale che controllano la massa muscolare. Interventi terapeutici mirati a mantenere l'equilibrio dei processi di fusione e fissione mitocondriali possono, perciò, essere di fondamentale importanza per preservare la massa muscolare e prevenire l'atrofia.

1 INTRODUCTION

1.1 Skeletal muscle structure and function

The skeletal muscle is a very dynamic and plastic tissue, that accounts for almost 40% of total body mass and represents a major site of metabolic activity. Moreover muscles are responsible for body posture and movement, and are the protein reservoir of our organism. Skeletal muscle is composed by elongated and multinucleated cells called muscle fibers. Muscles fibers are organized in bundles and separated by a specific membrane system. Each muscle is surrounded by a connective tissue membrane called epimysium, and connected to the bones through the tendons. The muscle itself is formed by well organized bundles of muscle fibers that are grouped in fascicula and are surrounded by another layer of connective tissue, called perimysium. Within the fasciculus, each individual muscle fiber is surrounded by connective tissue called the endomysium (Figure 1) (Light and Champion, 1984).

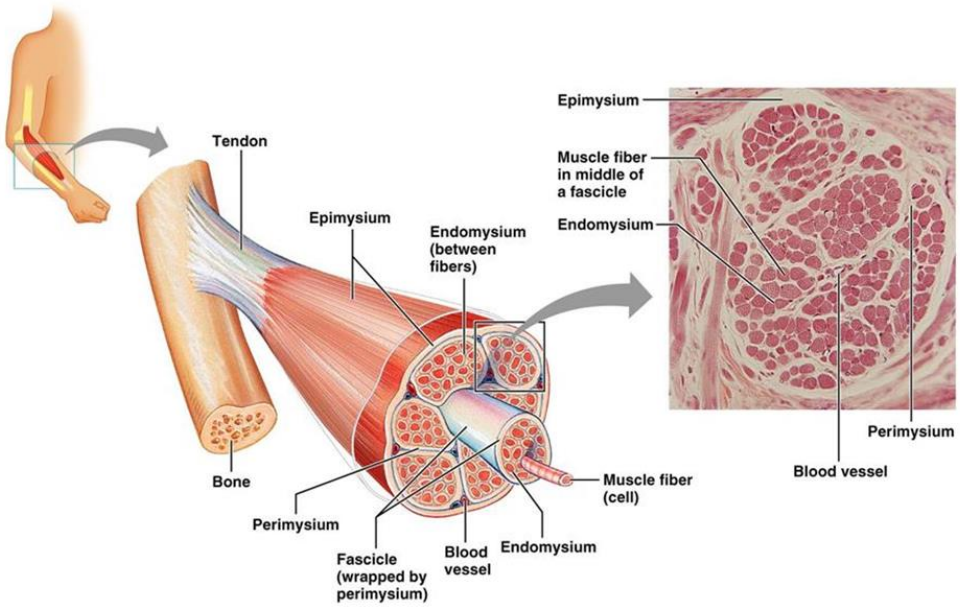

***Figure 1**: Schematic representation of skeletal muscle structure.*

Each muscle fiber contains a large number of myofibrils that run parallel to its length. The myofibril contains the contractile elements of skeletal muscle cells. The unit of muscle contraction is called sarcomere, which is associated in series to form the myofibrils, and in parallel, thus generating the striated pattern of muscle fibers. Sarcomere structure was described first thank to microscopy techniques that individuated isotropic (light band) and anisotropic (dark band) zones, forming the specific striated aspect of the skeletal muscle. For this reason, sarcomere is usually defined as the segment between two neighbour Z-lines, that appears as a series of dark lines. Surrounding the Z-line, there is the region of the I-band (the light band). Following the I-band there is the A-band (the dark band). Within the A-band, there is a paler region called the H-band. Finally, inside the H-band there is a thin M-line, the middle of the sarcomere. These bands are not only morphological unit, but also functional, because they are characterized by the presence of different contractile proteins required for muscle contraction. In fact, actin filaments (thin filaments) are the major component of the I-band and extend into the A band. Myosin filaments (thick filaments) extend throughout the A-band and are thought to overlap in the M-line. A huge protein, called titin, extends from the Z-line of the sarcomere, where it binds to the thin filament system, to the M-line, where it is thought to interact with the thick filaments. Several proteins important for the stability of the sarcomeric structure are found in the Z-line as well as in the M-line of the sarcomere (Figure 2). Actin filaments and titin molecules are cross-linked in the Z-disc via the Z-line protein alpha-actinin. The M-line myosin as well as the M proteins bridge the thick filament system to the M-line part of titin (the elastic filaments). Moreover several regulatory proteins, such as tropomyosin and troponin bind myosin molecules, modulating its capacity of contraction (Barrett et al., 2010).

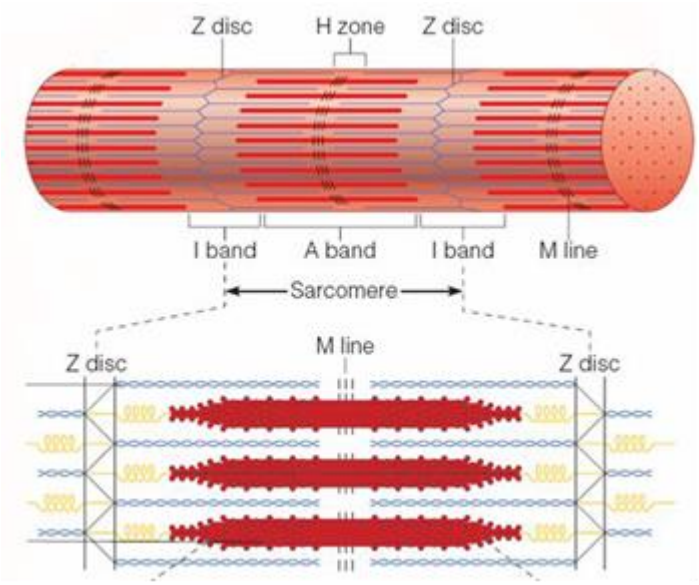

***Figure 2**: Schematic representation of skeletal muscle sarcomere.*

Muscle contraction is due to the excitation-contraction coupling, by which an electrical stimulus is converted into mechanical contraction. The general scheme is that an action potential arrives to depolarize the cell membrane. By mechanisms specific to the muscle type, this depolarization results in an increase in cytosolic calcium that is called a calcium transient. This increase in calcium activates calcium-sensitive contractile proteins that then use adenosine triphosphate (ATP) to cause cell shortening. Concerning skeletal muscle, upon contraction, the A-bands do not change their length, whereas the I bands and the H-zone shorten. This is called the sliding filament hypothesis, which is now widely accepted. There are projections from the thick filaments, called cross-bridges which contain the part (head) of myosin linked to actin. Myosin head is able to hydrolyse ATP and covering chemical energy into mechanical energy.

To allow the simultaneous contraction of all sarcomeres, the sarcolemma penetrates into the cytoplasm of the muscle cell between myofibrils, forming membranous tubules called transverse tubules (T-tubules) (Figure 3). The T-tubules are electrically coupled with the terminal cisternae which continue into the sarcoplasmic reticulum. Thus, the Sarcoplasmic Reticulum, which is the

enlargement of smooth Endoplasmic Reticulum (ER) and which contains the majority of calcium ions required for contraction, extends from both sides of T-tubules into the myofibrils. Anatomically, the structure formed by T-tubules surrounded by two smooth ER cisternae is called the triad and it allows the transmission of membrane depolarization from the sarcolemma to the ER. The contraction starts when an action potential diffuses from the motor neuron to the sarcolemma and then it travels along T-tubules until it reaches the sarcoplasmic reticulum. Here the action potential changes the permeability of the sarcoplasmic reticulum, allowing the flow of calcium ions into the cytosol between the myofibrils. The release of calcium ions induces the myosin heads to interact with the actin, allowing the muscle contraction. The contraction process is ATP-dependent. The energy is provided by mitochondria which are located closed to Z line (Barrett et al., 2010).

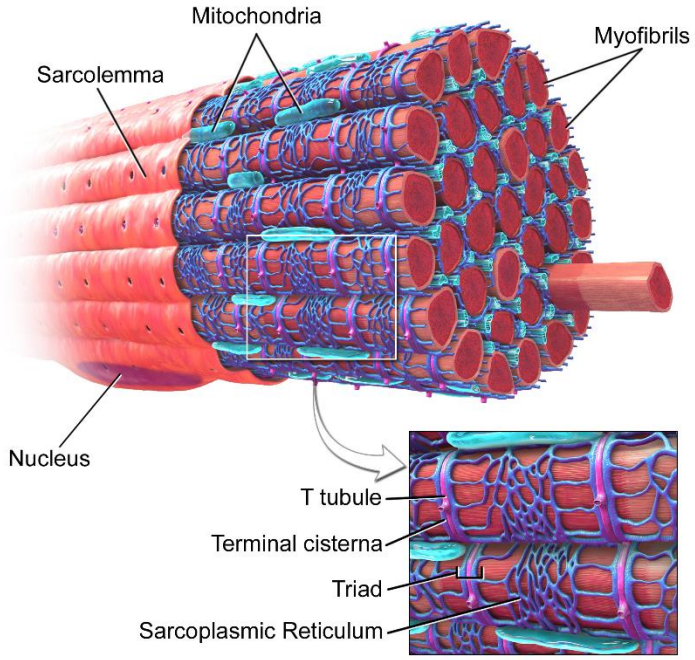

Figure 3: *Schematic representation of T-tubules and mitochondria in skeletal muscle.*

The contraction properties of a muscle depend on the fiber type composition. Mammalian muscle fibers are divided into two distinct classes: type I, also called slow fibers, and type II, called fast fibers. This classification considers only the mechanical properties. However, the different fiber types also show peculiar features such as for example myosin ATPase enzymes, metabolism (oxidative or glycolytic), mitochondrial content revealed by succinate dehydrogenase (SDH) staining, and resistance to fatigue (Pette and Heilmann, 1979; Schiaffino et al., 2007). It is possible to distinguish four major fiber types called I, IIA, IIX and IIB, based on the presence of different myosin heavy chain (MyHC) isoforms (Ciciliot et al., 2013). Fibers type I express the slow isoform MyHC-1 coded by MYH7 gene, and show a great content of mitochondria, high levels of myoglobin, high capillary density and oxidative capacity. For these reasons muscles containing many type I fibers appear red. Type IIA fibers express MyHC-2A, coded by MYH2 gene. IIA fibers are slower compared to type I, but faster than type IIX and IIB, and they exhibit an oxidative metabolism and a relative fatigue-resistance due to the rich mitochondria content (Schiaffino and Reggiani, 2011; Schiaffino and Reggiani, 1996). Given all these characteristics, IIA fibers are also termed fast oxidative fibers. The IIX fiber type, expressing MyHC-2X, and IIB fiber type, which expresses MyHC-2B, are called fast-glycolytic fibers and show a prominent glycolytic metabolism containing few mitochondria of small size, high myosin ATPase activity, the fastest rate of contraction and the highest level of fatigability.
The fiber-type profile of different muscles is initially established during development independently of neural influence, but nerve activity has a major role in the maintenance and modulation of its properties in adult muscle. Indeed during postnatal development and regeneration, a default nerve activity-independent pathway of muscle fiber differentiation, which is controlled by thyroid hormone, leads to the activation of a fast gene program. On the contrary, the post-natal induction and maintenance of the slow gene program is dependent on slow motoneuron activity. The muscle fiber-type then undergoes further changes during

postnatal life, for example fiber-type switching could be induced in adult skeletal muscles by changes in nerve activity (Murgia et al., 2000).

1.2 Muscle hypertrophy and atrophy

Maintenance of skeletal muscle mass is essential for health and survival. Skeletal muscle mass varies according to physiological conditions such as physical activity, metabolism and hormones, but also in many diseases. The regulation of muscle mass and fiber size depends on protein turnover, reflecting the balance between protein synthesis and degradation. In particular, muscle growth is mainly due to protein synthesis, that, when exceeds, leads to muscle hypertrophy. On the contrary, loss of proteins, organelles and cytoplasm are major causes of muscle atrophy.

1.2.1 Muscle hypertrophy

Skeletal muscle hypertrophy occurs during development, in response to mechanical overload and/or anabolic hormonal stimulation. During development the size of muscle fibers is controlled by cell turnover, which depends on satellite cells proliferation and fusion to muscle growth, and protein turnover. On the contrary in adulthood, the increase of muscle mass reflects an increased protein synthesis and concomitant a decrease in protein degradation.

Protein turnover is mainly regulated by a highly conserved pathway composed of IGF-1 and a cascade of intracellular effectors that include the kinases Akt/PKB and the mammalian target of rapamycin (mTOR). Muscle-specific IGF-1 overexpression in transgenic mice results in muscle hypertrophy and, importantly, the growth of muscle mass matches with a physiological increase of muscle strength. Furthermore, the overexpression of a constitutively active form of Akt in adult skeletal muscle induced muscle hypertrophy. Moreover, Akt transgenic mice display muscle hypertrophy and protection from denervation-induced atrophy, showing that this pathway promotes muscle growth and blocks protein degradation

(Schiaffino et al., 2013). Akt pathway, in fact, controls in an opposite manner two important downstream targets: mTOR and glycogen synthase kinase 3 beta (GSK3β). In the first case, Akt phosphorylates and activates the serine/threonine protein kinase mTOR, a master regulator of cell growth. mTOR promotes protein synthesis through the activation of the ribosomal protein S6 kinases 1 and 2 (S6K1 and S6K2) and blocking the inhibition of the initiation factor 4E binding protein 1 (4EBP1). In the other case, the inhibition of GSK3β from Akt stimulates proteins synthesis, since GSK3β normally blocks protein translation initiated by eIF2B protein (Glass, 2005). Moreover Akt can inhibit protein degradation through its action on FoxOs transcription factors, which activate proteolytic pathways. In conclusion, IGF-1-Akt axis is a major mediator of skeletal muscle hypertrophy. Recently, it has been reported that also myostatin and other members of the TGF-β pathway contribute to regulation of muscle mass in adulthood (Lee et al., 2004; Sartori et al., 2013). In particular, TGF-β pathway has a negative effect on muscle growth mediated by Smad2 and Smad3 transcription factors. Moreover, bone morphogenetic protein (BMP) signaling, acting through Smad1, Smad5 and Smad8 (Smad1/5/8), is one of the fundamental hypertrophic signals in mice. Sartori et al. demonstrated that when the BMP pathway is blocked or myostatin expression is increased, Smad4 binds to phosphorylated Smad2/3, leading to atrophy. On the contrary, a decrease in Smad2/3 phosphorylation levels, leads to the release of Smad4, which promotes hypertrophy through its binding to Smad1/5/8. Importantly, they identify a newly characterized ubiquitin-ligase, named MUSA1, as the molecular mechanism underlying the anti-atrophic action of the BMP pathway that has a negative effect on its expression. This work provided evidences that also BMP signalling is involved in the regulation of adult muscle mass in normal and pathological situations (Sartori et al., 2013).

1.2.2 Muscle atrophy

Muscle mass loss, named muscle atrophy, occurs in several pathological conditions like disuse, denervation, immobilization, sepsis, cancer, diabetes, AIDS, heart and renal failure and during aging. In 2004 it was demonstrated that all these catabolic states involve a common transcriptional program that includes the deregulation of a subset of genes involved in protein degradation, protein synthesis, reactive oxygen species (ROS) detoxification, UPR, energy production and growth-related processes. These groups of genes are called "Atrogenes" (Lecker et al., 2004). Muscle atrophy involves the shrinkage of myofibers due to a net loss of proteins. The ubiquitin-proteasome system (UPS) and the autophagy-lysosome pathway are the degradation systems involved in this process (Sandri, 2013).

1.2.3 Ubiquitin-Proteasome System

The ubiquitin-proteasome system is one of the major mechanism that control protein breakdown in skeletal muscle. In UPS, protein are targeted for the proteasomal degradation through the covalent binding of a poly-ubiquitin chain. This highly specific process consists of three sequential action involving distinct enzymes: E1 (ubiquitin-activating enzyme), E2 (ubiquitin-conjugating enzyme) and E3 (ubiquitin-protein-ligase) (Figure 4). Briefly, E3 binds the protein substrate and catalyzes the movement of the ubiquitin from E2 enzyme to the substrate. This is the rate-limiting step of the ubiquitination process, thus the amount and the type of proteins degraded by the proteasome is largely determined by which E3 ligases are activated in the cell (Gomes et al., 2001).

Among the known E3s, only a few of them are muscle specific and are upregulated during muscle loss (Sacheck et al., 2007). The first to be identified were Atrogin-1/MAFbx and MuRF1, which are specifically expressed in striated and smooth muscles (Bdolah et al., 2007; Bodine et al., 2001; Gomes et al., 2001). Atrogin-1 and MuRF1 expression is under the control of FoxOs transcription factors. FoxOs family members (FoxO1, FoxO3, FoxO4), which are target of Akt, are key

regulators of this catabolic process during muscle atrophy. Indeed the muscle-specific concomitant deletion of FoxO1/3/4 protects from muscle atrophy preventing the induction of several E3 enzymes, including Atrogin-1 and MuRF1 (Milan et al., 2015).

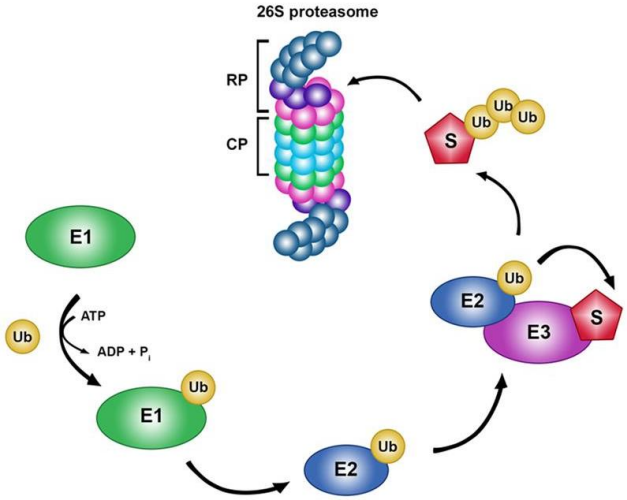

***Figure 4**: Schematic representation of the ubiquitination process.*

1.2.4 Autophagy-Lysosome System

Autophagy-lysosome system is a highly conserved catabolic process used for the degradation and recycling, through the lysosomal machinery, of bulk cytoplasm, long-lived proteins and organelles. Autophagy takes place both in constitutive conditions and in response to various stimuli, such as cellular stress, nutrient deprivation, amino acid starvation and cytokines (Mizushima and Komatsu, 2011). There are three different mechanisms involved in the delivery of the autophagic cargo to lysosomes: macroautophagy, chaperone-mediated autophagy and microautophagy.

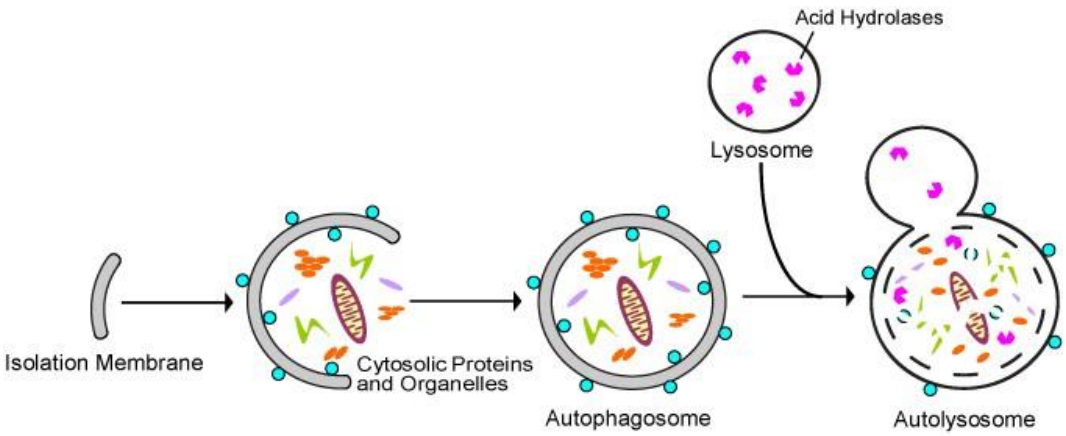

***Figure 5**: Representation of the different steps of the autophagic flux.*

The involvement of autophagy in muscle protein breakdown during atrophy was not recognized for a long time. It is now known that myofiber atrophy induced by *in vivo* overexpression of constitutively active FoxO3 requires autophagy, and siRNA-mediated knockdown of LC3 (a protein that contributes to autophagosome formation) partially prevents FoxO3-mediated muscle loss (Mammucari et al., 2007). Moreover, among atrogenes there are several genes belonging to the autophagy-lysosome system. Importantly, two autophagy genes, LC3 and Gabarap, which encode for proteins that are degraded when autophagosomes fuse with lysosomes, are two of the most upregulated atrogenes (Mammucari et al., 2008; Zhao et al., 2007).

During the autophagy process, the cargo that needs to be degraded is engulfed by double membranes layer called autophagosomes. These membranes have to be committed, and this requires the recruitment of ATGs proteins on the membrane. Autophagy-related genes (ATG) encode for proteins that mediate different steps of the autophagic process: initiation, elongation, maturation and fusion of the autophagosome with the lysosome, and cargo degradation (Tan et al., 2013). The elongation of the autophagosomal membranes is associated with ubiquitination-like reactions. In particular, microtubule-associated protein 1 light chain (Atg8/LC3) is conjugated to the autophagosome membrane on phosphatidylethanolamine (PE) with a covalent bond, by Atg7 (E1-like) and Atg3 (E2- like) to form LC3-II

(Rubinsztein et al., 2011). This modification results in a change of the molecular weight of LC3 that allows to distinguish by western blot the cytoplasmic soluble LC3-I, from the lipidated LC3-II isoforms. Usually, the accumulation of LC3-I or a decrease in LC3-II means that autophagy is blocked. Moreover, LC3 interact with p62, a scaffold protein involved in several signal transduction pathways. p62 binds to ubiquitinated proteins and in this way acts as a bridge between ubiquitinated proteins that have to be degraded, and LC3-II located in the inner membrane of the autophagosome. Since LC3-II in the inner autophagosomal membrane is degraded together with other cellular constituents by lysosomal proteases, p62 trapped by LC3 is transported selectively into the autophagosome, and the impaired autophagy is accompanied by accumulation of p62 (Ichimura and Komatsu, 2010). p62 is also required in the targeting to the autophagosomes of dysfunctional mytochondria, thus being involved in a specific selective autophagy process, called mitophagy.

Autophagy is mainly regulated by nutrient availability, so the Akt pathway is the major player in autophagy regulation. In condition of nutrient deprivation, in fact autophagy is activated, so the most potent autophagy inhibitor in skeletal muscle is Akt. In addition, acute activation of Akt in adult mice or in muscle cell cultures completely inhibits autophagosome formation and lysosomal-dependent protein degradation during fasting (Mammucari et al., 2007; Zhao et al., 2007; Zhao et al., 2008).

Autophagy needs to be properly regulated and genetic manipulations to activate or inhibit it results into muscle atrophy (Mammucari et al., 2007; Masiero et al., 2009; Romanello et al., 2010). These evidences demonstrated that basal autophagy is essential for skeletal muscle homeostasis, while impairment in the autophagic flux leads to muscle atrophy and weakness.

1.3 Role of mitochondria in skeletal muscle homeostasis

Mitochondria are double-membrane organelles characterized by two membranes that have different properties. The composition of the OMM is similar to the

eukaryotic one, whereas the inner mitochondrial membrane (IMM) resembles prokaryotic membranes in its physical properties and composition (Scorrano, 2013). Mitochondria not only are involved in ATP production, but they participate in many other metabolic pathways that include calcium homeostasis and cell death. Skeletal muscle mass is determined by a balance of protein synthesis and degradation. Both systems requires ATP, which is provided by mitochondria. Importantly, more than 10% of the atrophy-related genes are directly involved in energy production and are strongly downregulated in different atrophy models. In fact, several genes encoding for enzymes important in glycolysis and oxidative phosphorylation are coordinately suppressed in atrophying muscles (Lecker et al., 2004). Moreover, during muscle contraction energy requirements increases instantaneously up to 100-fold the consumption of ATP (Blei et al., 1993; Gaitanos et al., 1993). These findings underline the key role of mitochondria in the maintenance of muscle mass and function.

Several reports identified that there are two different mitochondrial population within myofibers: the intermyofibrillar (IMF) mitochondria located between the contractile filaments, and the subsarcolemmal (SS) mitochondria which are located underneath the sarcolemma. SS mitochondria represent 20% of mitochondria within skeletal muscle and IMF mitochondria account for the remaining 80% (Hoppeler, 1986). These two populations have different functional and biochemical properties. SS mitochondria have a large lamellar shape and provide energy for membrane-related events. In contrast, IMF mitochondria are smaller and supply ATP for muscle contraction. All these mitochondria are not isolated organelles, but they form an interconnected network that adapts to cellular needs in order to respond immediately to changes in energy requirement (Romanello and Sandri, 2016).

1.4 Mitochondria-shaping machinery

Mitochondria are dynamic organelles that rapidly change size, number and morphology depending on a balance between two opposite processes: fusion and fission. Both mechanisms are evolutionarily conserved from yeast to humans. Fusion and fission processes are essential for embryonic development, apoptosis, calcium signaling and determination of lifespan, and are affected in several human genetic diseases. In addition, in the last years, we learned that changes in mitochondrial shape influence crucial cellular function including generation of ROS, neuronal plasticity, lymphocyte migration and muscle atrophy (Campello and Scorrano, 2010). Mitochondrial fusion leads to the formation of an interconnected network facilitating the redistribution of metabolites, proteins and mtDNA. Moreover fusion prevents the local accumulation of defective mitochondria. Conversely, fission generates isolated and fragmented mitochondria allowing the removal of dysfunctional and damaged organelles via mitophagy. When mitochondria divide, two organelles are generated, one with high membrane potential that might undergo fusion, and another fragment with low membrane potential and reduced optic atrophy 1 (Opa1) levels that will not rejoin the mitochondrial network and will be likely removed by autophagy (Twig et al., 2008).

1.4.1 Fusion machinery

When mitochondria fuse they follow a scheme which starts with mitochondria tethering, continues with fusion of OMM and concludes with fusion of IMM (Romanello and Sandri, 2016). The two dynamin-related GTPases mitofusin1 (Mfn1) and mitofusin2 (Mfn2) are the principal regulators of OMM fusion in mammals (Santel and Fuller, 2001). Both mitofusins are integrated into the OMM and can interact homotypically (Mfn1-Mfn1, Mfn2-Mfn2) or heterotypically (Mfn1-Mfn2) to promote tethering and fusion of adjacent mitochondria. The proteins have a high degree of homology, but they do not have the same functions.

Indeed, Mfn2 is expressed also on SR facilitating the interaction with mitochondria. In this way Mfn2 plays an important role in calcium homeostasis (de Brito and Scorrano, 2009).

Opa1, another dynamin-like GTPase, is required for the fusion of the IMM. There are several splicing variants of Opa1, 8 in humans and 4 in mice, which are expressed in a tissue specific manner. Moreover Opa1 is regulated by different post-transcriptional modifications that include the cleavage of long Opa1 isoforms (Opa1L) into short Opa1 isoforms (Opa1S) that are represented experimentally by five bands on a Western Blot. Fusion requires both long and short isoforms. Interestingly, Opa1 has other functions: it is involved in the regulation of apoptosis controlling cristae remodeling and cytochrome c release (Germain et al., 2005; Frezza et al., 2006), and it controls the assembly of respiratory chain complexes (RCC) into supercomplexes (Cogliati et al., 2013).

1.4.2 Fission machinery

Mitochondrial fission depends on the cytosolic GTPase dynamin-related protein 1. Drp1 shows a cytosolic localization and is recruited to the OMM of damaged mitochondria where it assembles into multimeric ring complexes that form active GTP-dependent mitochondrial fission sites (Smirnova et al., 2001). Drp1 translocation to mitochondria depends on adaptor proteins on the OMM that act as receptors. Fis1 is the major receptor in yeasts (Karren et al., 2005). Fis1 overexpression triggers mitochondrial fission, whereas its downregulation promotes mitochondrial elongation, even if the recruitment of Drp1 to mitochondria is not reduced (Lee et al., 2004). Recently other Drp1 receptors have been discovered: mitochondrial fission factor (Mff) and mitochondrial division (MiD; MiD49 and MiD51). Mff colocalizes with Drp1 on mammalian mitochondria and its ablation causes mitochondrial elongation. MiD49 and MiD51 are N-terminal-anchored OMM proteins that form foci or ring-like structures on mitochondria and are involved in the recruitment of Drp1 onto mitochondria (Palmer et al., 2011).

1.4.3 Drp1 structure and regulation

Drp1 is an 80 kDa protein which belongs to a family of large GTPases that self-assemble into spirals using the hydrolysis of GTP to change its conformation. Indeed Drp1 oligomerizes in a GTP-dependent manner into helices that wrap around mitochondria. Drp1 protein structure (Figure 6) includes an amino-terminal GTPase domain, a middle domain, and a GTPase effector domain (GED) (Elgass et al., 2013). The levels of Drp1 mRNAs are high in brain, moderate in skeletal and heart muscles, and low in other tissues, including liver, kidney, placenta, and lung (Smirnova et al., 1998).

Drp1 is regulated by several post-translation modifications like ubiquitination, phosphorylation, SUMOylation, and S-nitrosylation to ensure a rapid adaptation to cellular needs (Otera et al., 2013). Phosphorylation of different residues of Drp1 cause opposing effects. For example, during mitosis Drp1 activity is promoted by Cdk1-cyclin B-dependent phosphorylation at Ser616 in GED (Taguchi et al., 2007). Fission is induced also by the phosphorylation of Ser637 in the GED promoted by the calcium/calmodulin-dependent protein kinase I alpha (CaMKI alpha). However, phosphorylation of the same residue by the protein kinase A (PKA) has an opposite effect causing Drp1 retention in the cytosol (Cribbs and Strack, 2007). This inhibition is counteracted by calcineurin-dependent dephosphorylation.

Mitochondrial fission is also stimulated by sumoylation of Drp1 by the SUMO E3 ligase mitochondria-anchored protein ligase (MAPL) (Braschi et al., 2009). Finally, Drp1 can be ubiquitinated by Parkin and MARCHV/Mitol E3 ubiquitin ligases.

A final Drp1 modification recently described is S-nitrosylation. This modification by nitric oxide (NO) triggers mitochondrial fission.

***Figure 6**: Drp1 protein structure.*

1.5 Mitochondrial dysfunction and muscle atrophy

Among the genes that are dysregulated during muscle wasting, there are genes encoding key enzymes for ATP and glycolysis (Lecker et al., 2004). Accordingly, alterations in mitochondria morphology and function were found also in several wasting conditions including cancer cachexia (Antunes et al., 2014), insulin resistance (Crescenzo et al., 2014), and different neuromuscular disorders (Katsetos et al., 2013). Over the last years, several *in vivo* study highlighted the importance of mitochondrial morphology and mitochondrial dysfunction signaling in the activation of nuclear programs controlling muscle loss (Romanello and Sandri, 2016). So, the maintenance of balanced fusion/fission processes is necessary to preserve muscle mass and prevent muscle wasting.

1.5.1 Mitochondrial fusion and atrophy

The biological importance of mitochondrial dynamics in early development is revealed by the embryonic lethality of mouse knock-outs for Opa1, Mfn1, and Mfn2 (Chen et al., 2003; Davies et al., 2007). Importantly, muscle-specific knock-out mice for Mfn1 and Mfn2 are viable at birth, although they display important muscle atrophy and mitochondrial dysfunction (Chen et al., 2010). However, very little is known about the role of fusion machinery in skeletal muscle *in vivo*.

Loss of function mutations in Mfn2 and Opa1 causes Charcot-Marie-Tooth type 2A (CMT2A) and dominant optic atrophy (DOA) respectively. Both CMT2A and DOA are neurodegenerative diseases characterized by muscle atrophy and myopathy.

Further support in the role of mitochondrial fusion in the maintenance of muscle mass comes from genetic models of controlled Opa1 overexpression. Indeed, Opa1 transgenic mice are protected from acute muscle loss induced by denervation (Varanita et al., 2015) as well as chronic muscle loss in a model of myopathy (Civiletto et al., 2015).

1.5.2 Mitochondrial fission and atrophy

Impairment in mitochondrial fission triggers the accumulation of dysfunctional organelles that are detrimental for cells. Indeed, mutations in mitochondrial fission components can be lethal. An infant girl born with a dominant-negative mutation of Drp1 presented alterations in brain development and in metabolism that cause neonatal lethality (Waterham et al., 2007). Likewise, mice lacking Drp1 have embryonic and brain development abnormalities and died after embryonic day 11.5-12.5 (Ishihara et al., 2009; Wakabayashi et al., 2009). Moreover genetic perturbations leading to the ablation of Drp1 in heart or brain are lethal (Ishihara et al., 2009; Wakabayashi et al., 2009; Kageyama et al., 2014; Ikeda et al., 2015; Song et al., 2015).

In skeletal muscle, atrophying conditions are characterized by alterations of the mitochondrial network (Romanello et al., 2010). Furthermore the acute overexpression of the fission machinery in skeletal muscle is sufficient to induce mitochondrial dysfunction and muscle atrophy via the activation of ubiquitin-proteasome and autophagy-lysosome systems (Romanello et al., 2010). A recent report demonstrated also that constitutive muscle-specific overexpression of Drp1 leads to muscle mass loss and decreased exercise performance (Touvier et al., 2015).

1.5.3 Mitophagy and Atrophy

Mitochondria are the major source of ROS that may oxidize mitochondrial lipids, proteins and DNA (Scherz-Shouval et al., 2010). High ROS levels are detrimental for cellular function and can induce damage to contractile proteins and organelles in skeletal muscle (Carnio et al., 2014). So, the maintenance of a functional mitochondrial network is particularly important for tissues that are highly structured and metabolically active such as neurons, cardiac and skeletal muscles (Romanello and Sandri, 2016). Since post-mitotic tissues cannot dilute damaged and dysfunctional mitochondria through mitosis, they depend only on the activation of mitochondrial quality controls pathway to avoid cell damage. The selective removal of mitochondria via autophagy, named mitophagy, has emerged as a key mechanism in this quality control, allowing the removal of mitochondria that are irreversibly damaged (Kanki et al., 2010). In mammals the loss of mitochondria membrane potential causes mitophagy. The selective removal of mitochondria depends on a set of proteins including PINK1, Parkin, Bnip3L/Nix, and Bnip3. Bnip3 and Nix are essential for mitophagy, indeed they promote the tethering of mitochondria to autophagosome acting as autophagy receptors. In fact, these proteins interact with LC3 and Gabarap through conserved LIR (LC3 interacting region) domains.

Also Parkin mediates the selective engulfment of depolarized mitochondria by autophagosome (Narendra et al., 2008). Parkin is recruited on damaged mitochondria by the mitochondrial kinase PINK1. Usually PINK1 is rapidly degraded in healthy mitochondria, whereas it accumulates on the surface of dysfunctional organelles. When Parkin translocates to damaged mitochondria, it catalyzes the ubiquitination of several proteins on OMM, that are then recognized by the autophagy receptor p62. Moreover since the damaged organelle that is going to be degraded by autophagosome needs to fit into his forming structure, mitophagy depends on mitochondria fragmentation (Gomes and Scorrano, 2013). Indeed disrupted mitochondrial fission, obtained with cardiac-specific ablation of Drp1, induces accumulation of defective mitochondria due to impaired

autophagy/mitophagy, that over-time promotes cardiomyocyte death (Kageyama et al., 2014).

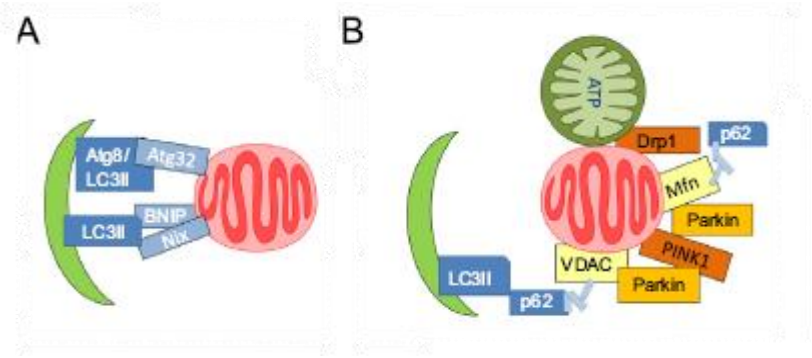

***Figure** 7: Mitochondrial recruitment during mitophagy: (A) Atg32 in yeast, NIX and BNIP in mammals bind mitochondria that has to be degraded, (B) moreover mitophagy can be stimulated by mitochondrial fission through Drp1 activation (adatpted Dodson et al., 2013).*

The accumulation of damaged mitochondria which can release ROS is deleterious for myofiber health. Indeed, the deletion of Atg7, a crucial autophagy gene, in skeletal muscle leads to the accumulation of abnormal mitochondria, oxidative stress, and apoptosis that result in muscle atrophy (Masiero et al., 2009). Accordingly, muscle-specific Atg5 knock-out mice displayed a similar phenotype (Raben et al., 2008). Moreover, dysregulation of the autophagic flux is a common feature of a group of muscle disorders with alterations of lysosomal proteins such as Danon or Pompe Disease (Sandri et al., 2013) and of muscular dystrophy caused by defects in collagen VI production (Grumati et al., 2010).

However, also an excessive increase of the autophagic flux can be deleterious for muscle homeostasis. For example, the transient overexpression of FoxO3, Bnip3, or Nix triggers mitochondrial dysfunction and muscle atrophy (Mammucari et al., 2007; Romanello et al., 2010). Therefore, autophagy and mitophagy need to be properly regulated. Indeed, constitutive basal autophagy is required to preserve mitochondrial function and skeletal muscle homeostasis.

1.5.4 Role of mitochondria in Sarcopenia

It has been shown that several mechanisms necessary for mitochondrial homeostasis are dysregulated during sarcopenia, the progressive age-related decline in muscle mass and force. Sarcopenic muscles are characterized by atrophy, weakness, denervation, and mitochondria dysfunction. The impairment in mitochondria functionality is the result of the decline in mitochondrial biogenesis and an accumulation of dysfunctional organelles that are not removed. Importantly, also the balance between fusion and fission is altered in sarcopenic muscles. Indeed, through transcriptomic and proteomic analysis, Glass and colleagues showed that muscles from 6, 18, and 27 months-old rats have a progressive loss of mitochondrial proteins involved in fusion and fission processes (Ibedunjo et al., 2013).

Also mitophagy has a central role in age-related mitochondrial defects. Indeed, the genetic ablation of Atg7 in skeletal muscle displays precocious aging characterized by increased oxidative stress, mitochondrial dysfunction, muscle mass loss and weakness, and degeneration of neuromuscular junction (Carnio et al., 2014).

1.6 Role of mitochondrial in Ca^{2+} signaling

Calcium (Ca^{2+}) is a highly versatile second messenger that controls different mechanisms such as neurotransmission and muscle contraction. Cellular Ca^{2+} homeostasis is mainly controlled by two organelles: ER and mitochondria. The ER is the major intracellular Ca^{2+} store of cells. Mitochondria, on the other hand, decode cellular Ca^{2+} signals by taking up and then releasing Ca^{2+} ions (Santo-Domingo and Demaurex, 2010). The release of Ca^{2+} into the cytosol is triggered by action potentials and/or by second messengers.

In skeletal muscle Ca^{2+} is stored inside SR, which is in close contact with T-tubules. Action potentials propagated through the T-tubular system are sensed by dihydropyridine receptors, which are located opposite to ryanodine receptors

(RyRs), the Ca^{2+} release channels present in the terminal cisternae of the SR, and this causes calcium release (Schneider, 1994).

The responsible for mitochondrial Ca^{2+} uptake is MCU which catalyzes the passive uptake of Ca^{2+} across the inner membrane of mitochondria, driven by the negative mitochondrial potential (Bernardi, 1999). MCU is a highly selective, low conductance Ca^{2+} channel (Kirichok et al., 2004). The discrepancy between the low affinity of MCU to Ca^{2+} and the rapid mitochondrial Ca^{2+} accumulation is due to close proximity of mitochondria to SR-resident Ca^{2+} channels. So, mitochondria location allows them to rapidly sense cellular Ca^{2+} signals and to act as highly localized buffers (Rizzuto et al., 2012). GFP labelling of ER and mitochondria revealed the presence of overlapping regions, called "Mitochondria Associated Membranes" (MAM), and the area of contact sites has been estimated as 5-20% of the total mitochondrial surface (Rizzuto et al., 1998).

In fast twitch fibers mitochondria are found mostly in correspondence of the I band, closely apposed to the SR, adjacent to triads. On the other hand, in slow twitch fibers mitochondria are also found in longitudinal clusters between myofibrils and under the sarcolemma (Ogata and Yamasaki, 1985). The positioning of mitochondria close to sites of Ca^{2+} release in skeletal muscle fibers provides a physical basis for excitation-metabolism coupling and localized SR-mitochondrial Ca^{2+} signaling (Rossi et al., 2008). Moreover, mitochondria influence SR-Ca^{2+} release by controlling the redox state of RyR. Indeed, oxidation-dependent modification of RyR by mitochondrial ROS, increases probability of channel opening, leading to dysfunction in SR Ca^{2+} release/reuptake. In addition, SR Ca^{2+} leak increases mitochondrial Ca^{2+} uptake leading to mitochondrial Ca^{2+} overload, which in turn leads to increased ROS production. The increase in oxidative stress promotes RyR leak, resulting in a "vicious cycle" whereby SR Ca^{2+} leak and mitochondrial ROS are locally amplified and lead to progressive age-dependent muscle dysfunction (Durham et al., 2008; Andresson et al., 2011).

Mitochondrial calcium uptake modulates also the activity of several dehydrogenases (pyruvate dehydrogenase, isocitrate dehydrogenase, oxoglutarate

dehydrogenase) and carriers (McCormack et al., 1990). The results of the increased mitochondrial calcium (Ca^{2+}_{mit}) content is a higher respiratory rate. However, mitochondrial Ca^{2+} uptake need to be precisely controlled because the prolonged increase in mitochondrial Ca^{2+} can induce the opening of the mitochondrial permeability transition pore (PTP) leading to mitochondrial swelling and apoptosis. Indeed, mitochondrial Ca^{2+} uptake can profoundly influence cell survival and various functions, such as metabolism and signaling. Another fundamental Ca^{2+}_{mit}-dependent process concerns the control of autophagy. In particular, Ca^{2+} has a role as inhibitor of autophagy: when the physiological Ca^{2+}_{mit} uptake is abolished, an increase in the AMP/ATP ratio is registered, with a consequent AMPK activation, which stimulates autophagy (Cardenas et al., 2010).

The large change in ATP requirements that underlines muscle activity renders Ca^{2+} transfer to mitochondria a key signaling step in skeletal muscle. A clear indication of the importance of MCU-dependent mitochondrial Ca^{2+} accumulation in skeletal muscle function was the recent identification of a mutation of MICU1, a direct modulator of MCU, in patients with proximal muscle weakness, learning difficulties, and extrapyramidal motor disorder (Logan et al., 2014). Moreover, the $MCU^{-/-}$ mice show clear metabolic and functional alterations of skeletal muscle (Pan et al., 2013).

Mammucari and coworkers investigated the role of MCU in skeletal muscle by overexpressing or silencing MCU. The results show that MCU overexpression triggers hypertrophy by controlling protein synthesis. On the contrary, a decrease in MCU protein expression reduces markedly skeletal muscle fiber size. Moreover MCU exerts a protective effect against atrophy highlighting the importance of mitochondrial Ca^{2+} signaling for the maintenance of skeletal muscle trophism (Mammucari et al., 2015).

1.7 Aim of the work

The maintenance of a functional mitochondrial network is particularly important for tissues that are highly structured and metabolically active such as neurons, cardiac and skeletal muscles. It is known that fusion and fission processes are involved in the preservation of mitochondria functionality. These mechanisms are of fundamental importance in post-mitotic tissues, such as skeletal muscle. In particular, mitochondria fission is necessary for the fragmentation and the removal of damaged organelles via mitophagy. A failure of this system leads to the accumulation of dysfunctional mitochondria and predisposes to organ dysfunction and degeneration. Moreover, alterations in mitochondria number and morphology are associated with muscle wasting and contribute to the loss of muscle mass during aging. However, little is known about the role of mitochondria fission in skeletal muscle *in vivo*. For this reason we wanted to determine whether genetic manipulation of mitochondrial fission proteins influences muscle mass. So, in order to investigate the importance of this process in muscle homeostasis, my PhD project is focused on the characterization of the role of Drp1 in skeletal muscle. We therefore generated a conditional muscle-specific Drp1 knock-out mouse model ($Drp1^{-/-}$ MLC). Moreover, consistent with the crucial role of mitochondria dynamics in post-mitotic tissues, the conditional deletion of Drp1 in brain and cardiomyocytes lead to lethality. Therefore, we generated a muscle-specific inducible Drp1 deficient mouse model ($Drp1^{-/-}$ HSA). This second model allowed us to investigate the physiological and pathological role of Drp1 in adulthood. In addition, we wanted to unravel the retrograde signal that from mitochondria affects myonuclear gene expression.

2 MATERIALS AND METHODS

2.1 Animal handling and generation of muscle-specific Drp1 knock-out mice

Animals were handled by specialized personnel under the control of inspectors of the Veterinary Service of the Local Sanitary Service (ASL 16 - Padova), the local officers of the Ministry of Health. All procedures are specified in the projects approved by the Italian Ministero Salute, Ufficio VI (authorization numbers 1060/2015PR). Muscles were removed at various time periods and frozen in liquid nitrogen for subsequent analyses.

Conditional muscle-specific $Drp1^{-/-}$ mice were obtained by crossing mice bearing *Drp1* floxed alleles with transgenic mice expressing Cre recombinase under the control of Myosin Heavy Chain 1 fast promoter (MLC1f-Cre), that is expressed only in skeletal muscle during the embryonic development (Bothe et al., 2000). Experiments were performed on newborns at post-natal day 12. Cre-negative littermates were used as controls.

To obtain inducible muscle-specific Drp1 knock-out mice, floxed Drp1 mice were crossed with mice carrying Cre-ER driven by the human skeletal actin promoter (HSA) (Schuler et al., 2005). Tamoxifen-induced Cre LoxP recombination was activated by oral administration of tamoxifen-containing chow (Tam400/Cre-ER Harlan), which was administered for 5 weeks. Muscles were collected 5 weeks after the tamoxifen diet finished. Adult mice (3 to 5 months-old) of the same sex and age were used for each individual experiment.

2.1.1 Genotyping of muscle-specific Drp1 knock-out mice

Mice were identified by analysing the presence of Cre-recombinase on genomic DNA by PCR. DNA was extracted using a lysis buffer containing Tris-HCL 1M

pH 7.5 and Proteinase K 10mg/mL (Life Technologies). The samples were denatured by incubation for 1 hour at 57°C and then the proteinase K was inactivated at 99°C for 5 minutes. For the PCR reaction we used the following primers:

Cre Forward - NSP-780: CACCAGCCAGCTATCAACTCG

Cre Reverse - NSP-979: TTACATTGGTCCAGCCACCAG

We prepared a 20µl total volume mix for each sample with:

Template DNA: 2µl

Primer NSP-780 (10µM): 0.2µl

Primer NSP-979 (10µM): 0.2µl

GoTaq Green master mix 2X (Promega): 10µl

Water

Program:

step 1: 94° C for 3 minutes
step 2: 94° C for 45 seconds
step 3 61° C for 30 seconds
step 4 72°C 1 minute
step 5: go to step 2 for 40 times

We detected Cre-recombinase DNA (200 bp) with a 2% agarose gel.

The genotyping analysis of Drp1 floxed allele were performed by using the following primers:

Drp1 Forward: CAGCTGCACTGGCTTCATGACTC

Drp1 Reverse: GTCAACTTGCCATAAACCAGAG

2.2 *In vivo* FDB electroporation

Electroporation experiments were performed on FDB muscles from wildtype and knock-out animals. The animals were anesthetized by an intraperitoneal injection of xylazine (Xilor) (20mg/Kg) and Zoletil (10mg/Kg). 7µl of Hyaluronidase (2mg/ml) (Sigma-Aldrich) were injected in the feet of anesthetized mice to soften muscle tissue underneath the epidermis. After 50 minutes we injected 15µg of plasmid DNA (D1ER Cameleon; mt-Keima probe; shRNA against MCU) and after 10 minutes electric pulses were applied by two stainless needles placed at 1cm from each other (100V/cm) (100 Volts/cm, 20 pulses, 1s intervals). Muscles were analysed 10 days later. No evidence of necrosis or inflammation were observed after the transfection procedure.

2.3 *In vivo* muscle force measurements

Gastrocnemius muscle force was measured in living animals as previously described (Blaauw et al., 2008). We performed this experiment in collaboration with Bert Blaauw (VIMM, Padova). Briefly, mice were anesthetized and muscle contractile performance was measured *in vivo* using a 305B muscle lever system (Aurora Scientific Inc.). Contraction was elicited by electrical stimulation of the sciatic nerve. The torque developed during isometric contractions was measured at stepwise increasing stimulation frequency, with pauses of at least 30 seconds between stimuli to avoid effects due to fatigue. Duration of the trains never exceeded 600ms. Force was normalized to the muscle mass as an estimate of specific force. Animals were then sacrificed by cervical dislocation and muscles were dissected, weighted and frozen.

2.4 Measurement of *in vivo* protein synthesis

In vivo protein synthesis was measured by using the SUnSET technique (Goodman et al., 2011; Schmidt et al., 2009). Mice were anesthetized and then given an intraperitoneal injection of 0.040µmol/g puromycin dissolved in 100µl of PBS. At exactly 30 min after injection, muscles were collected and frozen in liquid nitrogen for Western Blot analysis. A mouse IgG2a monoclonal anti-puromycin antibody (clone 12D10, 1:5000) was used to detect puromycin incorporation.

2.5 Colchicine treatment

We monitored autophagic flux in basal condition using colchicine (Ju et al., 2010). Briefly, inducible transgenic mice were treated with 0,4mg/kg of colchicine or vehicle by intraperitoneal injection. The treatment was repeated twice every 12 hours prior to muscle harvesting.

2.6 FDB single fiber isolation

Animals were sacrificed through cervical dislocation, and FDB muscles collected with their tendons and put in a tube with collagenase (3mg/ml GIBCO-Life Technologies) in DMEM (GIBCO-Life Technologies) for 30 minute on ice and then 1 hour at 37° C for digestion. Meanwhile coverslip are coated with 10% matrigel (BD) in Tyrode's buffer. After digestion the muscles were removed from collagenase, washed to inactivate the collagenase and dissected.

2.7 Mitochondrial membrane potential analysis

Mitochondrial membrane potential was measured in isolated fibers from FDB muscles as previously described (Mammucari et al., 2007; Zhao et al., 2007). Briefly, FDB myofibers were placed for 15 minutes at 37°C in 1ml Tyrode's buffer

and loaded with 2,5nM Tetramethylrhodamine (TMRM) (Molecular Probes), a fluorescent lipophilic cationic molecule that accumulates in mitochondria in a potential-dependent manner. The solution contains also glucose (3,5g/l), to sustain the fibers during the experiment, and Cyclosporin H (8mM) (Enzo Life Science), to block mitochondrial pumps, that would transport TMRM outside the mitochondria. Myofibers were then observed at Olympus IMT-2 inverted microscope (Melville, NY) equipped with a CellR imaging system. Sequential images of TMRM fluorescence were acquired every 60s with a 4X 0.5 UPLANSL N A objective (Olympus). At the times indicated by arrows, oligomycin (Olm, 5μM) (Sigma-Aldrich) or the protonophore carbonyl cyanide-p-trifluoromethoxyphenylhydrazone (FCCP, 4μM) (Sigma) were added to the cell culture medium. We used oligomycin to inhibit ATP-synthase, because ATP-synthase can reversely transport protons across the inner mitochondrial membrane, so maintaining the potential also in dysfunctional mitochondria. For this reason, only this treatment allow us to detect real dysfunctional mitochondria, that would inevitably dissipate the potential, loosing TMRM signal. Images were acquired, stored and analysis of TMRM fluorescence over mitochondrial regions of interest was performed using ImageJ software (http://rsb.info.nih.gov/ij/).

2.8 Measurement of Mitochondrial DNA Copy Number

Total gastrocnemius DNA was isolated using Puregene Cell and Tissue Kit (Qiagen) and was amplified using specific primers for mtCOXII and 18S by real-time PCR using the Power SYBR Green RT-PCR kit (Applied Biosystems). The mtDNA copy number was calculated using 18S amplification as a reference for nuclear DNA content. Real-Time PCR was performed with the following primers:

18S Fw: CATTCGAACGTCTGCCCTATCA
18 S Rw: GGGTCGGGAGTGGGTAATTTG

COXII Fw: GCCGACTAAATCAAGCAACA
COXII Rw: CAATGGGCATAAAGCTATGG

2.9 Mito-mKeima mitophagy assay

Mitochondria-targeted mKeima plasmid (mt-Keima) (MBL International) was used to monitor mitophagy in transfected FDB single fibers. mt-Keima is a coral-derived protein that exhibits both pH-dependent excitation and resistance to lysosomal proteases. These properties allow rapid determinations to whether the protein is in mitochondria or the in lysosome (Katayama et al., 2011; Sun et al., 2015). In fluorescence microscopy, ionized Keima is detected as a red fluorescent signal at acidic pH (lysosome) and neutral Keima as a green fluorescent signal at higher pH (mitochondria) (Proikas-Cezanne and Codogno, 2011). Fluorescence of mt-Keima was imaged in two channels via two sequential excitations (458 nm, green; 561 nm, red) and using a 570- to 695-nm emission range. The level of mitophagy was defined as the total number of red pixels divided by the total number of all pixels.

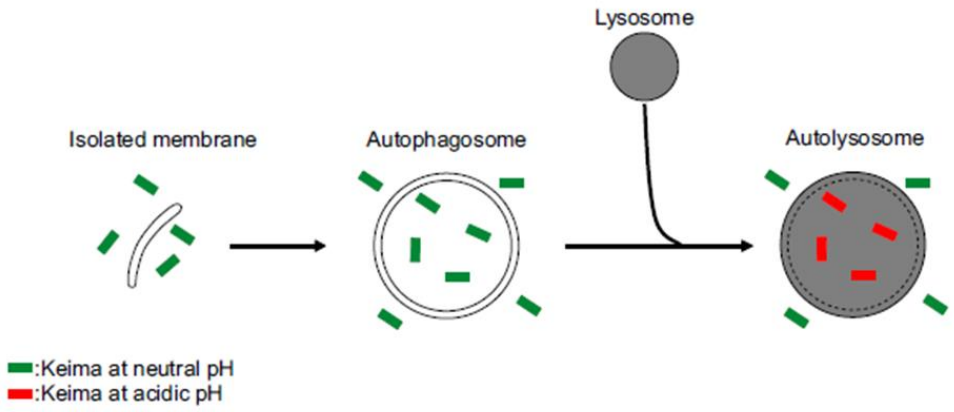

Figure 1: *Keima-based probe changes color upon conversion of an autophagosome to an autolysosome (Katayama et al., 2011).*

2.10 Calcium homeostasis analysis

All these experiments were done in collaboration with Prof. Reggiani (Physiology Department, University of Padua) and Prof. Rizzuto (Department of Biomedical Sciences, University of Padua).

2.10.1 Cytosolic calcium determination with FURA-2AM

Fibers were loaded with 5μM Fura-2 AM (Molecular Probes, Invitrogen) as described previously (Paolini et al., 2007), washed twice for 10 minutes with incubation buffer without BSA at 37°C to retain the indicator in the cytosol, and immersed in imaging buffer. After a minimum of 30 minutes, calcium signals were recorded using a dual-beam excitation fluorescence photometry setup (IonOptix Corp.) at 25°C. Fibers were electrically or chemically stimulated following the protocol described below. Ca^{2+} measurements were expressed as fluorescence Ratio of the emission at 480 nm with reference to the excitation wavelengths of 360 and 380 nm, respectively. Calibration of the Fura-2 AM signals and calculation of the free cytosolic calcium concentration were previously reported (Canato et al., 2010).

2.10.2 Electrical stimulation

In order to study calcium homeostasis under physiological condition of contractile activity, fibers were submitted to electrical stimulation. Fibers bathed with BTS 20μM to block spontaneous contraction at room temperature, then electrically stimulated with a train of pulses at 0.5 Hz with an amplitude of 20 V, followed by stimulation trains at higher frequency (60 Hz, 2 seconds).

2.10.3 Chemical stimulation

In order to mimic the electrical stimulation to study calcium transients, we took advantage of two chemical stimulators: caffeine and thapsigargin. Caffeine 20mM was used as an agent which stimulates Ca^{2+} release from SR through its action on RyR. Simultaneously, fibers were treated with thapsigargin 1μM, an inhibitor of the sarco/endoplasmic reticulum Ca^{2+} ATPase (SERCA). The stimulation of single fibers with caffeine and thapsigargin, that were directly added on cell medium, led to an increase in free calcium concentration that was detected with FURA-2AM in presence of EGTA 500μM.

2.10.4 Intra-SR calcium detection with D1ER

D1ER Cameleon FRET-based probe was used to measure SR calcium content. Fibers were prepared and stimulated as described above. SR free calcium levels were monitored using an inverted fluorescence microscope (Eclipse-Ti; Nikon Instruments). The excitation wavelength was 435 nm (10-nm bandwidth). YFP and CFP intensities were recorded by means of a cooled CCD camera (C9100-13; Hamamatsu) equipped with a 515 nm dichroic mirror at 535 nm (40 nm bandwidth) and 480 nm (30 nm bandwidth), respectively. YFP and CFP intensities were corrected for background by defining two corresponding regions of interest (ROIs) in each channel. Care was taken to select in both the YFP and the CFP image-corresponding regions of the fiber and background. The ratio (R) was defined as follows:

$$R = (YFP_{fiber} - YFP_{background}) / (CFP_{fiber} - CFP_{background})$$

Usually bleaching caused a slight decrease in the YFP signal and a minor increase in the CFP signal. This is an intrinsic feature of FRET-based probes, because bleaching of the acceptor leads to an increase in donor fluorescence. These opposite changes lead to a progressive slow decrease of the YFP/CFP ratio during the period of data acquisition. Correction for the change in baseline during the experiment was

performed by fitting a third-order polynomial through the initial and final 5s periods at the beginning and end of the recordings. The polynomial was subsequently subtracted from the recordings to remove time-dependent changes in the baseline and allow determination of the stimulation-dependent changes in the R (indicated as ΔR) and the measurement of their amplitude and time course (Canato et al., 2010).

2.11 *In vitro* mitochondrial assay

Mitochondria from WT and KO muscles were isolated as described (Frezza et al., 2007). To measure respiration, mitochondria (1mg/ml) were incubated in Experimental Buffer (EB: 150 mM KCl, 10 mM Tris Mops, 10 μM EGTA-Tris, 10μM ATP). Mitochondria were transferred into a Clark's type oxygen electrode chamber (Hansatech Instruments) and 5mM glutamate/2.5mM malate or 2μM rotenone/10mM succinate were added. Basal O_2 consumption was recorded and after 2 min 100μM ADP was added, followed by 2.5μg/ml oligomycin and 200μM FCCP. For complex IV dependent-O_2 consumption, mitochondria (1mg/ml) were incubated for the indicated time in EB supplemented with 5μM cytochrome c. Mitochondria were treated with 1nmol/mg Antimycin A and 2nM rotenone and they were transferred into a Clark's type oxygen electrode chamber. After 2 minutes 6mM Ascorbate and 300μM TMPD were added and the Complex IV-dependent O_2 consumption rate was measured. This set of experiments were done in collaboration with Prof. Scorrano (Biology Department, University of Padua).

To detect respiratory chain supercomplexes (RCS), Blue Native PAGE was performed by resuspending mitochondrial pellets in Native Blue buffer (Invitrogen) plus 4% Digitonin (Sigma) to a final concentration of 10μg/μl and incubated for 1 hour on ice. After 20 minutes of centrifugation at 16,000 g, the supernatant was collected and one-third of digitonin percentage of Sample Buffer 5% G250 (Invitrogen) was added. 50μg of mitochondrial membrane proteins were loaded and run on a 4-12% Bis-Tris gel (Invitrogen) as described in the NativePAGE™

Novex® Bis-Tris gel System manual. Western blot was performed using a Trans-Blot transfer cell (Bio-Rad) at 4°C overnight. List of antibodies is reported in Table1. This set of experiments were done in collaboration with Prof. Salviati (Biology Department, University of Padua).

2.12 Histology analyses and fiber size measurements

Muscles were collected and directly frozen by immersion in liquid nitrogen. Then we cut muscle 10μm thick cryosections by using Cryostat (Leica CM 1950). TA cryosections, were used to analyse tissue morphology with different methods, reported below. Images were collected with an epifluorescence Leica DM5000B microscope, equipped with a Leica DFC300-FX digital charge-coupled device camera, by using Leica DC Viewer software.

2.12.1 Haematoxilin and Eosin staining (H&E)

Haematoxylin colours basophilic structures that are usually the ones containing nucleic acids, such as ribosomes, chromatin-rich cell nuclei, and the cytoplasmic regions rich in RNA. Eosin colours eosinophilic structures bright pink. The eosinophilic structures are generally intracellular or extracellular protein.
The methods consist of:

Materials	Time
Harris Haematoxylin (Sigma-Aldrich)	1 minute
Wash in running tap water	2 minutes
Eosin Y Solution Alcoholic (Sigma-Aldrich)	1 minute
Ethanol 50%	30 seconds

Ethanol 70%	30 seconds
Ethanol 100%	5 minutes
Ethanol 100%	10 minutes
Xilen	3 minutes
Mount with Eukitt (Sigma-Aldrich)	

2.12.2 SDH staining

The succinate dehydrogenase is an enzyme complex localized in the inner mitochondrial membrane. This staining is used to evaluate approximately the quantity and the distribution of mitochondria present in the muscle fibers, through colorimetric evaluation. The reaction gives a purple coloration in the oxidative fibers, while the glycolytic fibers remain white. The sections were incubated for 30 minutes at 37°C with SDH solution (0.2M sodium succinate) (Sigma-Aldrich), 0.2M phosphate buffer (Sigma) pH 7.4 and 50mg of nitro blue tetrazolium (NBT) (Sigma-Aldrich). After the incubation, the sections were washed 3 minutes with PBS and then mounted with Mounting medium (Dako).

2.12.3 Fiber cross-sectional area (CSA)

Fiber CSA was measured, by using ImageJ software (National Institutes of Health). All data are expressed as the mean±SEM (error bars). Comparisons were made by using t test, with $p<0.05$ being considered statistically significant.

2.13 Immunoblotting

Cryosections of 20µm of TA muscles were lysed with 100µl of a buffer containing 50mM Tris pH 7.5, 150mM NaCl, 10mM MgCl2, 0.5mM DTT, 1mM EDTA, 10% glycerol, 2% SDS, 1% Triton X-100, Roche Complete Protease Inhibitor Cocktail and Sigma Protease Inhibitor Cocktail. After incubation at 70°C for 10 minutes and centrifugation at 11000 g for 10 minutes at 4°C, the surnatant protein concentration was measured using BCA protein assay kit (Pierce) following the manufacturer's instructions.

2.13.1 Protein gel electrophoresis

The extracted proteins from TA muscle were solubilized in Loading buffer composed by 5µl of 4X NuPAGE® LDS Sample Buffer (Life Technologies) and 1µl of 20X DTT (Life Technologies). The volume of each sample was brought to 20µl with SDS 1X. The samples were denatured at 70°C for 10 minutes. Samples were loaded on SDS 4-12% precast polyacrylamide gels (NuPAGE Novex-Bis-tris-gels) or in SDS 3-8% depending on the protein to be analyzed (Life Technologies). The electrophoresis was run in 1X MES/MOPS Running buffer or 1X Tris-Acetate Running buffer respectively (Life Technologies) for 1 hour and 30 minutes at 150V constant.

2.13.2 Transfer of the protein to the nitrocellulose membrane

After the electrophoretic run, proteins were transferred from gels to nitrocellulose membranes. The gel and the membrane were equilibrated in Transfer Buffer. The Transfer Buffer was prepared as follows: 50ml of 20X NuPAGE® Transfer buffer (Life Technologies), 1ml of 10X NuPAGE® Antioxidant (Life Technologies), 200ml of 20% Methanol (Sigma-Aldrich). The volume was brought to 1L with distilled water. The blotting was obtained by applying a current of 400mA for two

hours at 4°C. To evaluate the efficiency of the transfer, proteins were stained with Red Ponceau 1X (Sigma-Aldrich). The staining was easily reversed by washing with distilled water.

2.13.3 Incubation of the membrane with antibodies

Once the proteins were transferred on membranes, the membranes were saturated with Blocking Buffer (5% no fat milk powder or BSA solubilized in TBS 1X with 0.1% TWEEN) for 1 hour at room temperature and were incubated overnight with various primary antibodies at 4°C. Membranes were then washed 3 times with TBS 1X with 0.1% TWEEN at room temperature (RT) and incubated with secondary antibody-HRP Conjugate (Bio-Rad), for 1 hour at RT. Immunoreaction was revealed by SuperSignal West Pico Chemiluminescent substrate (Pierce) and followed by exposure to Xray film (KODAK Sigma-Aldrich). Blots were stripped using Stripping Solution, containing 25mM glycine and 1% SDS, pH 2.

Antibody	**Costumer**	**Dilution**
Rabbit anti-phospho-Akt (Ser473)	Cell Signaling #3787	1:1000
Rabbit anti-Akt	Cell Signaling #9272	1:1000
Rabbit anti-phospho-AMPK (Thr172)	Cell Signaling #2535	1:1000
Rabbit anti-AMPK	Cell Signaling #2532	1:1000
Rabbit anti-phospho-S6	Cell Signaling #2215	1:1000
Rabbit anti-S6	Cell Signaling #2217	1:1000
Rabbit anti-phospho-4EBP1 (Thr37/46)	Cell Signaling #9459	1:2000
Rabbit anti-phospho-4EBP1 (Ser65)	Cell Signaling #9455	1:1000
Rabbit anti-4EBP1	Cell Signaling #9452	1:2000

Mouse anti-BiP/GRP78	BD 610979	1:5000
Rabbit anti-phospho-eif2α	Abcam ab 32157	1:1000
Rabbit anti-eif2α	Cell Signaling #9722	1:1000
Rabbit anti-p62	Sigma P0067	1:2000
Rabbit anti-LC3	Sigma L7543	1:1000
Rabbit anti-Bnip3	Cell Signaling #3769	1:1000
Mouse anti-Drp1	BD 611738	1:2000
Mouse anti-GAPDH	Abcam ab8245	1:10000
Mouse anti-puromycin	Hybridoma Bank PMY-2A4	1:5000
Mouse anti-Porin	Santa cruz Sc-11415	1:10000
Rabbit anti-TOM20	Abcam ab14734	1:10000
Mouse anti-NDUFB8	Mol Probes 459210	1:5000
Mouse anti-CORE2	Mitoscience MS304	1:5000
Mouse anti-COXI	Mitosciences MS404	1:5000
Goat anti mouse IgG	Biorad 1706516	1:2000
Goat anti rabbit IgG	Biorad 1706515	1:2000

Table1*: Antibodies used for Western Blot analysis.*

2.14 Gene expression analysis

2.14.1 Extraction of RNA

Total RNA was isolated from gastrocnemius muscle using Trizol (Life Technologies) following the manufacturer's instructions.

2.14.2 Synthesis of the first strand of cDNA

400ng of total RNA was reversely transcribed with SuperScript^{TM} III (Life Technologies) in the following reaction mix:

Random primer hexamers (50ng/µl random): 1µl
dNTPs 10mM: 1µl
The volume was adjusted to 13µl with RNase-free water.

The samples were mixed and briefly centrifuged and denatured by incubation for 5 minutes at 65°C to prevent secondary structures of RNA. Samples were incubated on ice and the following components were added sequentially:

First strand buffer 5X (Life Technologies): 4µl
DTT 100mM: 1µl
Rnase Out (Life Technologes): 1µl
SuperScriptTM III (Life Technologies): 1µl
H_2O RNase-free: 0.5µl

The used reaction program was:

step1: 25°C for 10 minutes
step2: 42°C for 50 minutes
step3: 70°C for 15 minutes

At the end of the reaction, the volume of each sample was adjusted to 30µl with RNase free water.

2.14.3 Real-Time PCR reaction

Quantitative real-time PCR was performed with SYBR Green chemistry (Applied Biosystems). SYBR green is a fluorescent dye that intercalates into double-stranded DNA and produces a fluorescent signal. The real-time PCR instrument allows real-time detection of PCR products as they accumulate during PCR cycles and create

an amplification plot, which is the plot of fluorescence signal versus cycle number. In the initial cycles of PCR, there is little change in fluorescence signal. This defines the baseline for the amplification plot. An increase in fluorescence above the baseline indicates the detection of accumulated PCR products. A fixed fluorescence threshold can be set above the baseline. The parameter Ct (threshold cycle) is defined as the fractional cycle number at which the fluorescence passes the fixed threshold. So the higher the initial amount of the sample, the sooner the accumulated product is detected in the PCR process as a significant increase in fluorescence, and the lower is the Ct value.

1µl of diluted cDNAs was amplified in 10µl PCR reactions in an ABI Prism 7000 (Applied Biosystem) thermocycler, coupled with an ABI Prism 7000 Sequence Detection System (Applied Biosystems) in 96-wells plates (Micro Amp Optical, Applied Biosystems). In each well 5µl sample mix and 5µl reaction mix were mixed.
Sample mix was prepared as follows for 5µl total volume:

Template cDNA: 1 µl
H_2O Rnase-free: 4 µl

The SYBR Green qPCR (Applied Biosystem) was used for the real-time PCR reaction as follows:

SYBR Green qPCR (Applied Biosystem): 4.8µl
Mix Primer forward /reverse 50mM: 0.2µl

The PCR cycle used for the Real-Time PCR was:

step1: 95° C for 15 minutes
step2: 95° C for 25 seconds
step3: 58° C for 1 minute
step4: go to step 2 for 40 times

2.14.4 Quantification of the PCR products and determination of level of expression

A relative quantification method were used to evaluate the differences in gene expression, as described by Pfaffl (Pfaffl, 2001). In this method, the expression of a gene is determined by the ratio between a test sample and a housekeeping gene. The relative expression ratio of a target gene is calculated based on the PCR efficiency (E) and the threshold cycle deviation (ΔCt) of unknown samples versus a control, and expressed in comparison to a reference gene.

The mathematical model used for relative expression is represented in this equation:

$$\text{Ratio} = \frac{(E_{\text{target}})^{\Delta Ct}}{(E_{\text{reference}})^{\Delta Ct}}$$

The internal gene reference used in our real-time PCR was GAPDH, whose abundance did not change under the experimental conditions.

2.14.5 Primer pair design

Gene-specific primer pairs were selected with Primer Blast software (http://www.ncbi.nlm.nih.gov/tools/primer-blast/). Primer pairs were selected in a region close to the 3'-end of the transcript, and amplified fragments of 150-250bp in length. To avoid the amplification of contaminant genomic DNA, the target sequences were chosen on distinct exons, separated by a long (more than 1000bp) intron. The melting temperature was chosen to be of about 58-60° C. The sequences of the primer pairs are listed in Table 2.

	Forward primer (5'-3')	Reverse primer (3'-5')
Drp1	TCAGATCGTCGTAGTGGGAA	TCTTCTGGTGAAACGTGGAC
ATF4	TCCTGAACAGCGAAGTGTTG	ACCCATGAGGTTTCAAGTGC
GADD34	AGAGAAGACCAAGGGACGTG	CAGCAAGGAATGGACTGTG
CHOP	GCTGGAAGCCTGGTATGAG	ATGTGCGTGTGACCTCTGTT
FGF21	ATGGAATGGATGAGATCTAGA GTTGG	TCTTGGTGGTCATCTGTGTAGAG G
Atrogin1	GCAAACACTGCCACATTCTCTC	CTTGAGGGGAAAGTGAGACG
MuRF1	ACCTGCTGGTGGAAAACATC	ACCTGCTGGTGGAAAACATC
MUSA1	TCGTGGAATGGTAATCTTGC	CCTCCCGTTTCTCTATCACG
Smart1	TCAATAACCTCAAGGCGTTC	GTTTTGCACACAAGCTCCA
Fbxo31	GTATGGCGTTTGTGAGAACC	AGCCCCAAAATGTGTCTGTA
Trim37	ACACTGAGAACGAGGACAG	CAACAAATTTCAGGGACCAG
Itch	CCACCCACCCCACGAAGACC	CTAGGGCCCGAGCCTCCAGA
Beclin1	TGGAAGGGTCTAAGACGT	GGCTGTGGTAAGTAATGGA
LC3	CACTGCTCTGTCTTGTGTAGGT TG	TCGTTGTGCCTTTATTAGTGCATC
Bnip3	TTCCACTAGCACCTTCTGATGA	GAACACCGCATTTACAGAACAA
p62	CCCAGTGTCTTGGCATTCTT	AGGGAAAGCAGAGGAAGCTC
GabarapL	CATCGTGGAGAAGGCTCCTA	ATACAGCTGGCCCATGGTAG
CathepsinL	GTGGACTGTTCTCACGCTCAAG	TCCGTCCTTCGCTTCATAGG
GAPDH	CACCATCTTCCAGGAGCGAG	CCTTCTCCATGGTGGTGAAGAC

***Table 2**: Primer used for quantitative PCR analysis.*

IGF-1 quantification was performed using TaqMan® Universal PCR Master Mix and the specific TaqMan primers IGF1 class II (Mm 00439559_m1, Life Technologies). Data were normalized to GAPDH expression (Mm 99999915_g1, Life Technologies). Results are expressed as mean±SEM.

2.15 Serum glucose and FGF21 quantification

Blood was collected from the orbital sinus in heparin-coated Pasteur pipettes and centrifuged immediately after collection. Blood glucose levels were detected using Contour® blood glucose meter (Bayer).

Blood FGF21 levels were determined using Rat/Mouse FGF21 Enzime-linked Immunosorbent ELISA-Kit (Millipore, EZRMFGF21-26K) and following the manufacturer's instruction. Drp1 knock-out mice FGF21 relative quantification was normalized to controls. Data are expressed as fold increase of controls.

2.16 Statistical analysis

Survival probability evaluated by using Kaplan-Meier method. Comparison of controls and $Drp1^{-/-}$ survival curves was performed by both Mantel-Cox and Gehan-Breslow-Wilcoxon tests.

Generally, to reduce the standard deviation, we minimized physiological variation by using homogenous animals with same sex and same age. Comparisons were made by using two-tail Student's t-test, with $p \leq 0.05$ considered statistically significant. For all graphs data are represented as mean±SEM.

3 RESULTS

PART I

3.1 Generation of muscle-specific Drp1 knock-out mice

Dynamin related protein Drp-1 is required for mitochondrial fragmentation, a process essential in post-mitotic tissues. Furthermore, in our laboratory it was demonstrated that overexpression of mitochondrial fission machinery in adult muscle is sufficient to induce muscle atrophy (Romanello et al., 2010). However, little is known about the physiological role of Drp1 in skeletal muscle *in vivo*. For this reason we generated muscle-specific Drp1 knock-out mice, which are hereafter referred to as Drp1$^{-/-}$.

Drp1 floxed mice were crossed with a transgenic line expressing Cre recombinase (CRE) under the control of MLC1f promoter (Bothe et al., 2000) to generate mice lacking Drp1 in skeletal muscle from the birth (Drp1$^{-/-}$ MLC). We checked the successful deletion of Drp1 by quantitative RT-PCR analyses from RNA extracted from skeletal muscle (Fig. 1A). This result was confirmed by Western Blot analyses which shows that Drp1 protein is decreased in knock-out muscles, but not in other tissues including the heart (Fig. 1B).

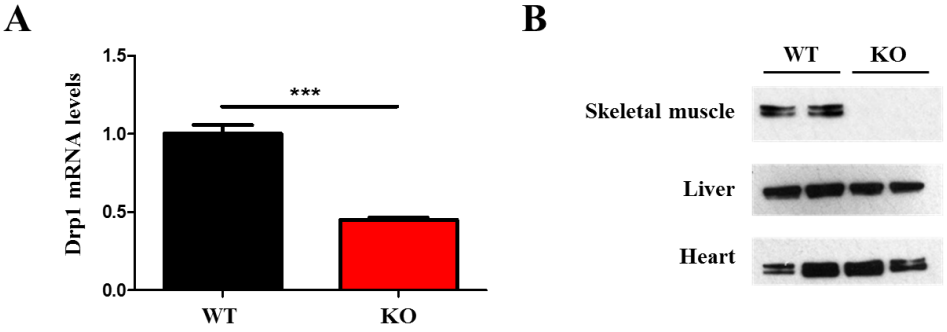

Figure 1: Validation of Drp1 knock-out model. A) *Drp1 mRNA expression levels analyzed by RT-PCR in muscles of Drp1$^{-/-}$ and control mice. n=7 mice each group.* ***B)*** *Representative Western Blot analyses shows that Drp1 protein levels in Drp1$^{-/-}$ is downregulated specifically only in skeletal muscle and not in other tissues. n=3 mice each group. ***p≤0.001.*

3.2 Skeletal muscle-specific deletion of Drp1 results in a lethal phenotype and muscle atrophy

We found, surprisingly that the specific ablation of Drp1 in skeletal muscle results in a lethal phenotype. Indeed, all Drp1$^{-/-}$ mice died within 30 days of postnatal life (Fig. 2A).

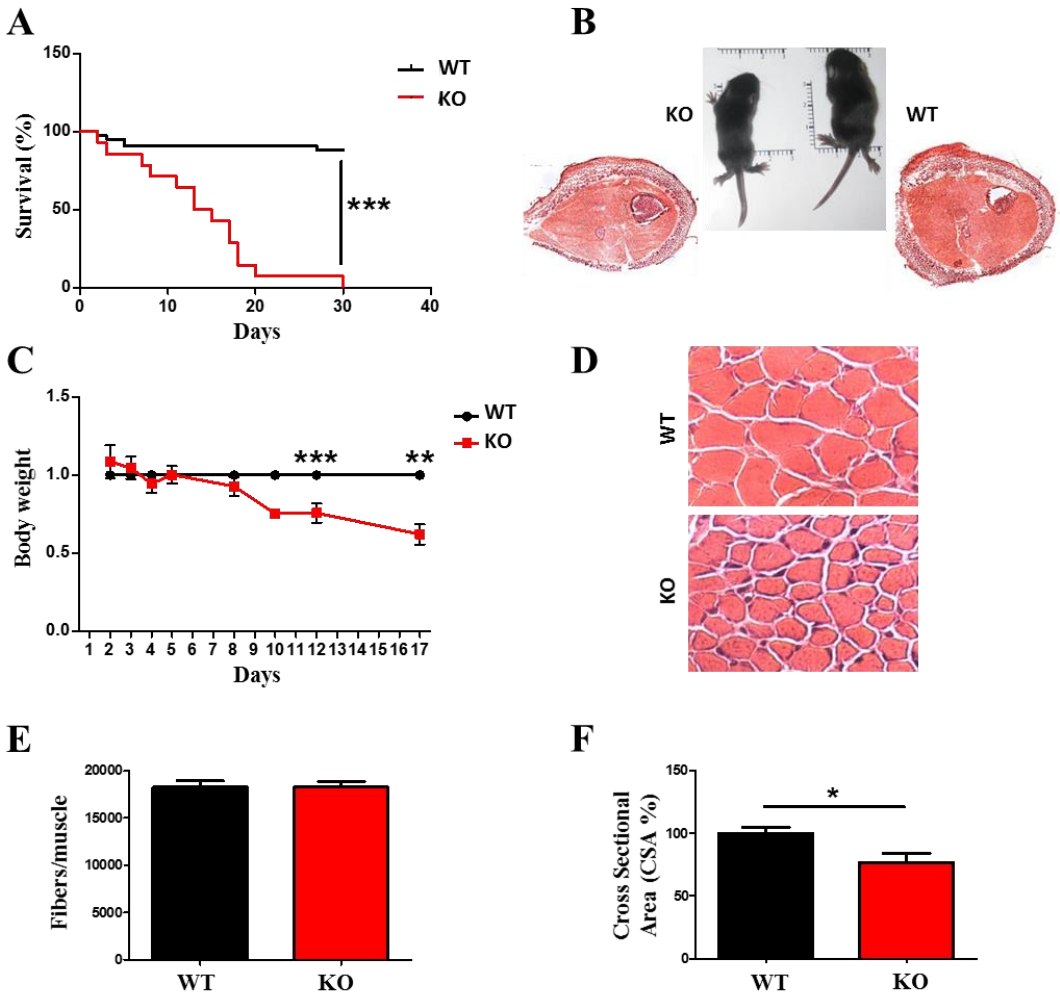

Figure 2: Drp1 ablation causes lethality and impairs muscle growth. ***A)*** *Kaplan-Meier survival curve of WT and KO littermates (WT n=37, KO n=15) indicates that deletion of Drp1 results in lethality.* ***B)*** *Upper panel: Representative photograph of control and KO littermates at post-natal day 12 showing that Drp1$^{-/-}$ mice are smaller than controls. Lower panel: Haematoxilin-Eosin (HE) staining of hindlimb cross-section.* ***C)*** *Drp1-deficient mice show an impairment in total body weight. n=10 animals for each condition.* ***D)***

Hematoxilin-Eosin staining shows that there are no signs of inflammation and degeneration. CSA analysis of fibers ***(F)*** *and total number analysis of fibers per muscle* ***(E)*** *indicate a reduction of Drp1 KO myofibers size without hypoplasia. Data represent mean ± SEM (F, n=6 mice each and E, n=3 mice each). *p≤0.05; **p≤0.01; ***p≤0.001.*

Moreover knock-out animals have a significant reduction in total body weight during the first 17 days of postnatal life leading to a smaller size despite the normal muscles and bones development (Fig. 2B, C). So, it is sufficient to delete a mitochondrial fission protein only in muscles to have an effect in the whole body metabolism.

Histological analysis of muscles at 12 days of postnatal life revealed a normal architecture and absence of myopathic features such as inflammation and centrally nucleated myofibers (Fig. 2D). In addition, total fiber number was conserved in $Drp1^{-/-}$ mice (Fig. 2E), while there was a reduction of about 25% in myofiber CSA (Fig. 2F). These data suggest that myogenesis and myotubes formation is not perturbed, but that postnatal myofiber growth is affected by Drp1 deletion.

3.3 *In vivo* protein synthesis is affected in Drp1 knock-out mice

In order to understand which is the mechanism that leads to decrease in fiber size, we studied protein synthesis in our mouse model. Muscle growth during the first two weeks of postnatal life depends on fusion of stem cell to growing myotube and on protein synthesis (Schiaffino et al., 2013). When we analyzed MyoD and myogenin expression, two markers of muscle stem cell proliferation and differentiation, we didn't find any differences confirming that myogenesis is not perturbed (Fig. 3A). So, we used SUnSET technique (Schmidt et al., 2009) to measure *in vivo* protein synthesis rate. Importantly, protein synthesis was reduced by 30% in $Drp1^{-/-}$ mice as shown by Western Blot analysis (Fig. 3B).

To understand such a reduction, we monitored the Akt/mTOR pathway in Drp1 deficient muscles. Interestingly, total 4EBP1, a downstream target of mTOR, was

increased and also hyper-phosphorylated in the Drp1$^{-/-}$ mice. Conversely, a second downstream mTOR target, S6, was significantly less phosphorylated in knock-out animals (Fig. 3C).

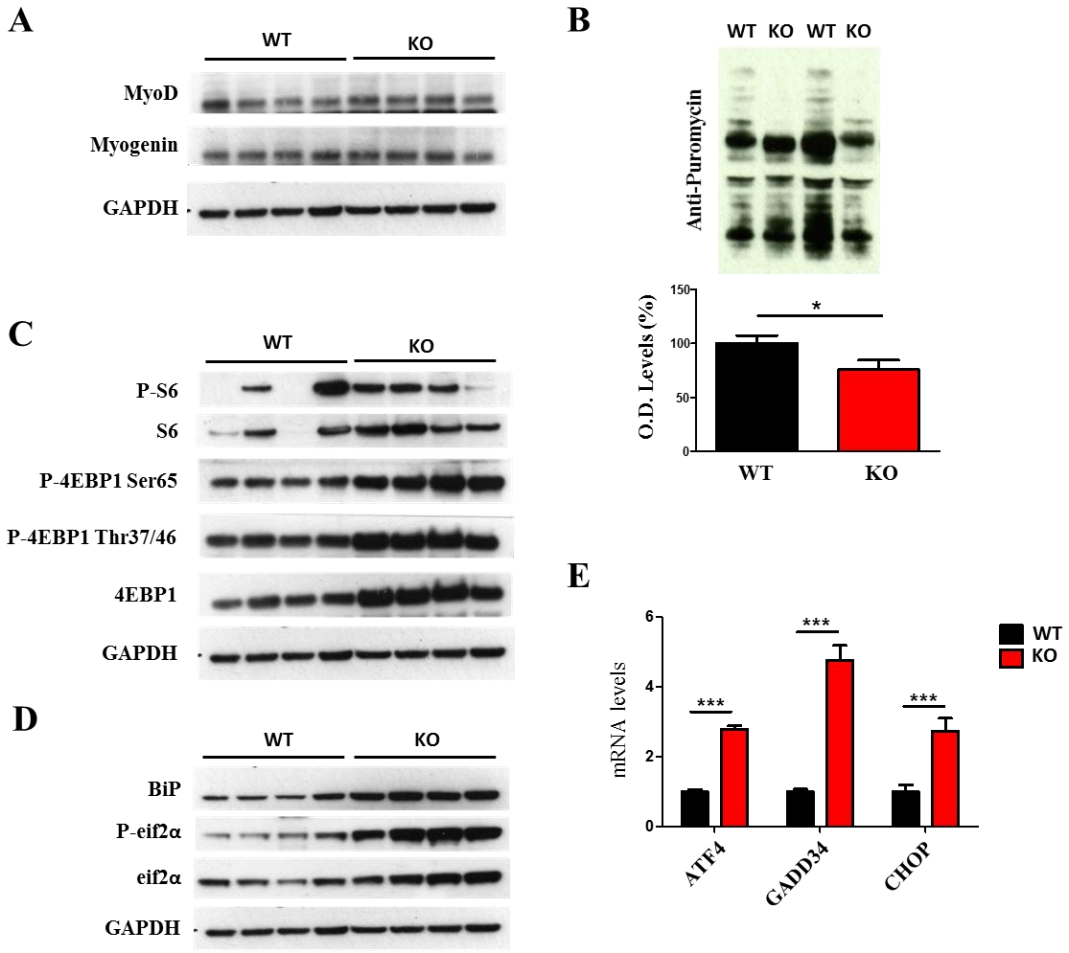

Figure 3: Drp1 absence leads to downregulation of protein synthesis and activation of UPR. A) *Representative immunoblot analysis of muscle homogenates of four WT and KO muscles. MyoD and Myogenin were normalized to GAPDH expression levels.* ***B)*** *In vivo SUnSET technique demonstrates a significant reduction of protein synthesis in Drp1-ablated muscles. Quantification of the puromycin-labeled peptides is expressed as percentage of the values obtained in the control group (n=8 mice).* ***C)*** *Total protein extracts from newborns muscles were immunoblotted with the indicated antibodies. n=8 each group.* ***D)*** *Western Blot analysis representing key players of the UPR pathway. All these proteins are induced in Drp1$^{-/-}$ muscles (n=8 mice).* ***E)*** *RT-PCR results confirming the activation of UPR pathway in absence of Drp1 (n=8 mice). *p≤0.05; ***p≤0.001.*

The incongruence of the Akt/mTOR/4EB1/S6 pathway suggests that other regulators are involved in the observed protein synthesis impairment. For this reason we decided to investigate the UPR pathway. UPR pathway through the kinase PERK phosphorylates eIF2α, a critical ribosome assembly initiation factor. When eIF2α is phosphorylated, the 43S complex cannot form anymore, ribosome assembly is blocked and general protein synthesis is shut down. In Drp1$^{-/-}$ muscles levels of p-eIF2α and of the chaperone BiP/Grp78, a downstream target of UPR, were significantly increased (Fig. 3D). Moreover, PERK-dependent unfolded protein response induces the activation of ATF4 transcription factor that is involved in the transcription of several genes including BiP, GADD34 and CHOP. All these genes, including ATF4, were upregulated in Drp1 null mice (Fig. 3E). In conclusion, UPR is strongly activated in knock-out animals and it is responsible for the translation impairment.

3.4 Unfolded Protein Response pathway leads to FGF21 secretion in plasma that lowers IGF-1 in the liver of knock-out mice

In mouse models of mitochondrial disease and in human patients, muscle fibers secrete FGF21, a fasting-related cytokine that enters the blood and goes in the circulation (Suomalainen et al., 2011; Tyynismaa et al., 2010). In addition, the skeletal muscle-specific Atg7 ablation leads to mitochondrial dysfunction and increases FGF21 through ATF4 (Kim et al., 2013). So, given the strong activation of ATF4 and UPR, we found that Drp1 ablation triggered FGF21 overexpression in skeletal muscles at 12 days of postanatal life (Fig. 4A). Importantly, FGF21 levels increased also in the blood of knock-out mice leading to a decreased glycaemia (Fig. 4B, C). In agreement, in a mouse model of impaired fatty acid oxidation in skeletal muscle, FGF21 was found to act in a paracrine manner to increase glucose uptake in muscle, lowering glycaemia (Vandanmagsar et al., 2016).

In 2008 it was demonstrated that FGF21 is able to downregulate GH action through STAT5 inhibition thus inhibiting serum IGF-1 (Inagaki et al., 2008). In our model, the deletion of Drp1 led to GH resistance and to the consequent decreased IGF-1 expression in liver (Fig. 4D). This might explain the smaller animal size.

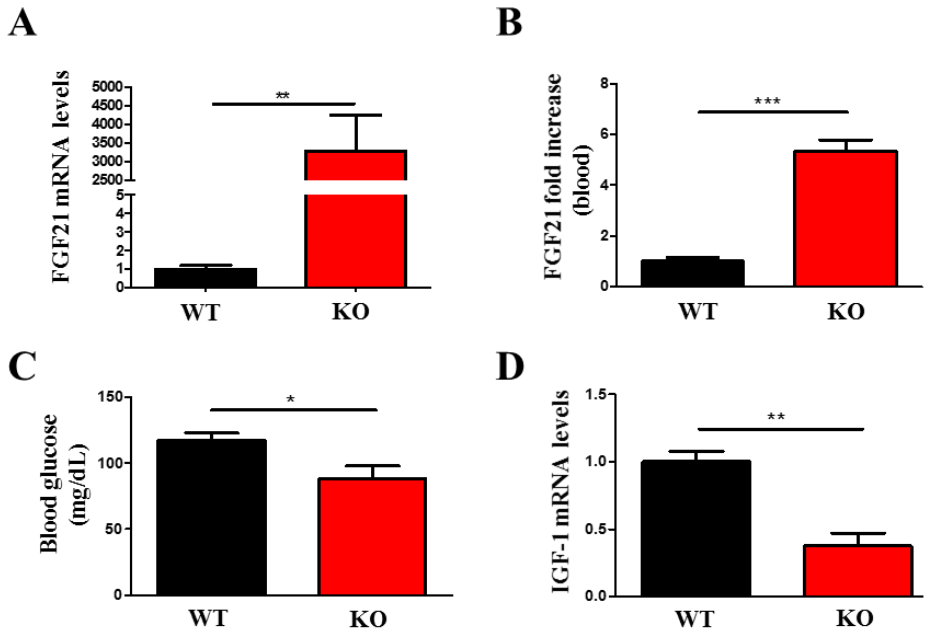

Figure 4: UPR leads to FGF21 overexpression that lowers IGF-1 levels in Drp1$^{-/-}$ muscles. A) *RT-PCR analysis reveal that FGF21 expression is increased upon Drp1 deletion (n=4 mice). Quantification of blood levels of FGF21 shows an increase in Drp1 KO mice (n=3), leading to a decrease in blood glucose (**C**, n=4 mice) and to a significant decrease in IGF-1 class II mRNA levels in the liver (**D**, n=4 mice). Statistical significance *p≤0.05; **p≤ 0.01; ***p≤0.001.*

3.5 Ubiquitin Proteasome and Autophagy-Lysosome systems are activated upon Drp1 deletion

Since the size of the cell is determined by the balance between protein synthesis and protein degradation, we also monitored ubiquitin-proteasome and autophagy-lysosome systems, the two main systems that control protein breakdown in skeletal

muscle. Protein degradation is characterized by a transcriptional-dependent program of atrogenes (or atrophy-related genes) (Lecker et al., 2004). These genes encode for enzymes that catalyze rate limiting steps during ubiquitination process and autophagosome formation. FoxOs-family members are the transcription factors involved in the regulation of several atrogenes. We measured by RT-PCR the expression levels of FoxO3 and of the atrophy-related E3 ubiquitin-ligases Atrogin1 and MuRF1. Both FoxO3 and the muscle-specific enzymes were upregulated in $Drp1^{-/-}$ mice compared to control (Fig. 5A). We also analyzed the transcription levels of a new set of ubiquitin-ligases named MUSA1 and Smart1, recently identified in our laboratory to be under FoxO regulation and involved in muscle atrophy (Sartori et al., 2013; Milan et al., 2015). Among them MUSA1 was induced in Drp1 knock-out animals (Fig. 5B). Then we monitored the expression of atrogenes involved in the autophagic-lysosomal system. Several of these genes implicated in different steps of the autophagic flux were induced in knock-out mice (Fig. 5C), confirming that an atrophy program was activated in this model. However, the ratio of LC3II (the lapidated form of LC3) on GAPDH was only mildly increased (Fig. 5D), while the levels of p62 did not change and there was a mild reduction on Bnip3 protein levels. These data suggest that autophagy was weakly induced in MLC-Drp1 knock-out mice. In conclusion, the deletion of Drp1 led to an impairment of postnatal muscle growth due to the inhibition in protein translation and to the activation of an atrophy program. All these features, in addition to IGF-1 decrease, contribute to the lethal phenotype.

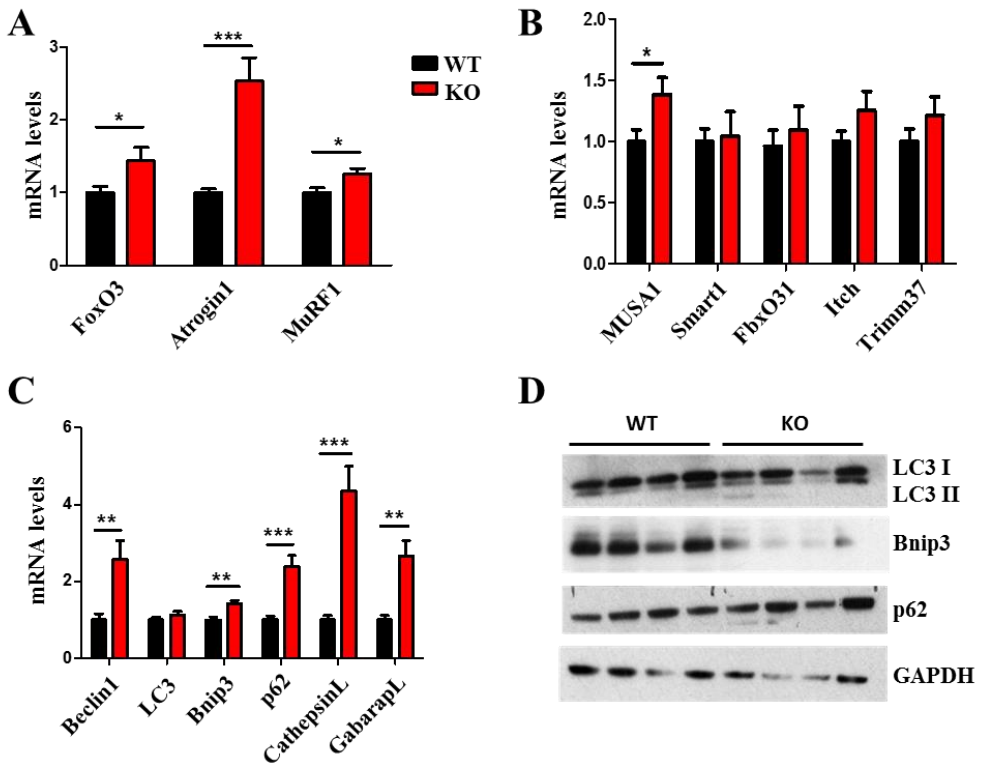

Figure 5: Drp1 absence leads to the activation of protein breakdown through Ubiquitin-Proteasome and Autophagy-Lysosome systems. ***A)*** *RT-PCR analysis shows an increased expression of FoxO3 and of the muscle-specific ubiquitin ligases Atrogin1 and MuRF1 and of the novel E3 enzyme MUSA1* ***(B)*** *in KO muscles. n=8 mice each condition.* ***C)*** *Quantitative PCR analysis of autophagy-related transcripts showing a significant induction of autophagy markers in Drp1$^{-/-}$ (n=8 mice).* ***D)*** *Representative immunoblots of four independent experiments of autophagy-related proteins. *p≤0.05; **p≤0.01; ***p≤0.001.*

PART II

3.6 Generation of muscle-specific inducible Drp1 knock-out animals

Considering the severity of MLC1f-Drp1 KO mice phenotype, we decided to investigate the role of Drp1 in muscle during adulthood. We therefore generated a tamoxifen-inducible muscle-specific Drp1 knock-out mouse model. This second knock-out model was obtained by crossing Drp1 floxed mice with mice carrying Cre-ER driven by the HSA promoter (Schuler et al., 2005). In these mice Cre recombinase (CRE) is fused with estrogen receptor and constantly degraded. When tamoxifen is administrated, it is able to bind to estrogen receptor thus preventing CRE degradation and promoting its nuclear localization. In this way tamoxifen treatment triggers the deletion of Drp1 only in skeletal muscle.

5 weeks of Tamoxifen treatment results in an efficient reduction of both transcript and protein levels in 5 months old Drp1$^{-/-}$ mice (Fig. 6A, B).

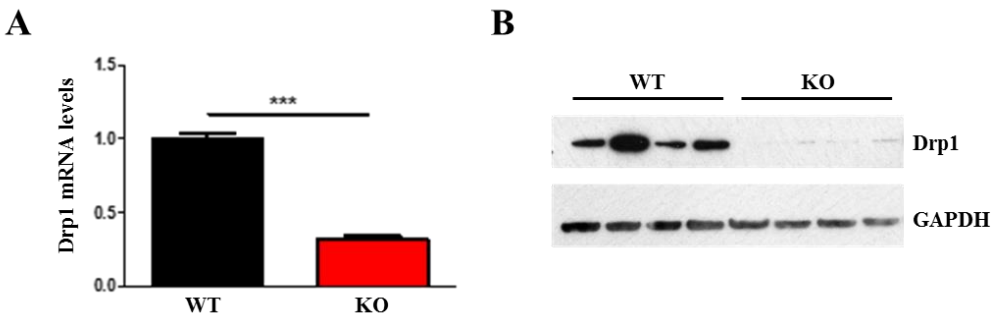

Figure 6: Generation of HSA-Drp1 knock-out mouse model. A) *Drp1 mRNA levels and Drp1 protein levels* ***(B)*** *are successfully downregulated in skeletal muscle of Drp1-null mice (n=6 mice each condition). *** p≤0.001.*

3.7 Acute deletion of Drp1 in adult mice causes body weight loss, muscle atrophy and weakness

When we monitored body weight of WT and KO mice during tamoxifen treatment, we noticed that knock-out animals started to spontaneously lose body weight within 50 days from the beginning of the treatment and during the following 3 weeks (Fig. 7A). The reduction of body weight was secondary to an important muscle mass loss, indeed skeletal muscles were significantly smaller in $Drp1^{-/-}$ mice compared to control (Fig. 7B). Moreover, quantification of fibers CSA showed that knock-out myofibers were 25% smaller than wildtype (Fig. 7C).

Morphological analyses of Tibialis Anterior revealed no features of inflammation or myofiber degeneration such as centre-nucleated fibers, suggesting that the decrease of muscle mass was due to atrophy (Fig. 7D). To understand if the reduction of myofiber area affected muscle performance, we analyzed *in vivo* strength of gastrocnemius muscle. Maximal absolute force (tetanic force) was significantly reduced in knock-out mice (Fig. 7E) indicating an increased loss of sarcomeric proteins. Importantly, also the specific force, the force normalized for muscle mass, was affected by Drp1 acute deletion (Fig. 7F).

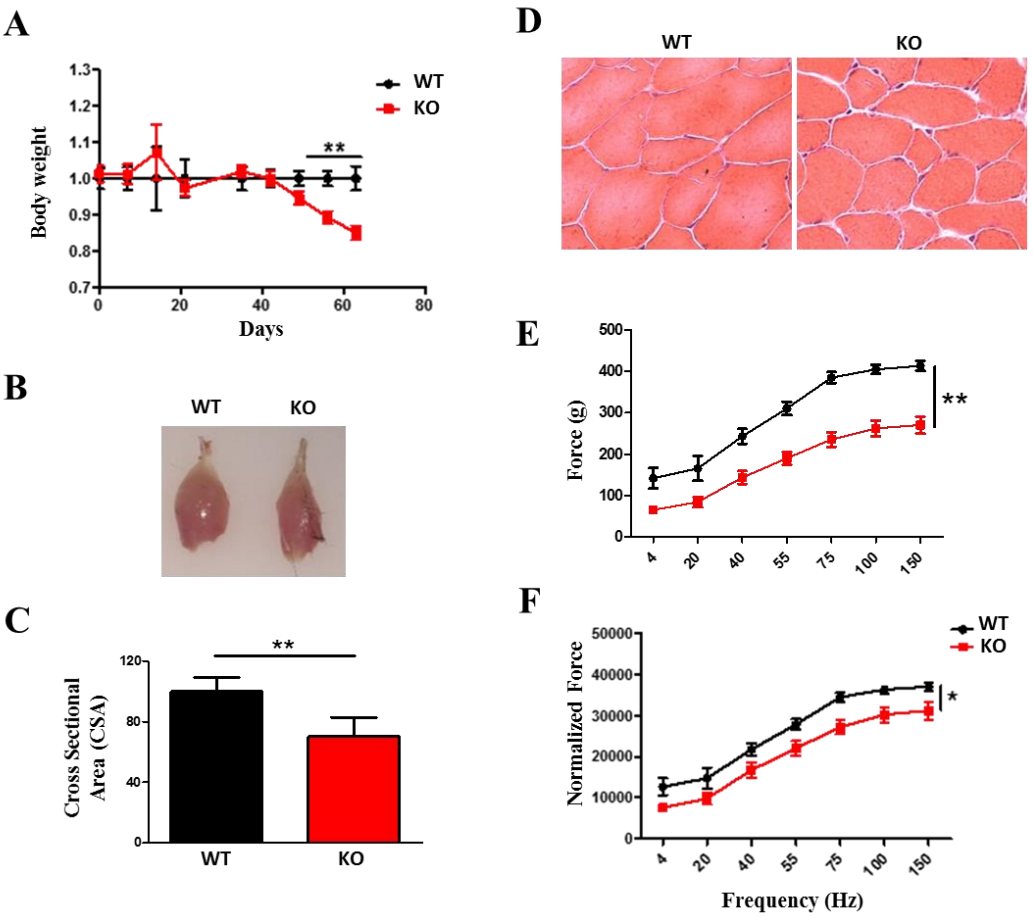

Figure 7: Deletion of Drp1 in adulthood results in muscle atrophy and weakness. A) *Body weight curve during and after tamoxifen treatment. KO mice start to loose body weight 7 weeks after the beginning of the treatment (WT n=10, KO n=11).* ***B)*** *Dissected gastrocnemius muscle from control and Drp1-deleted mice shows an important muscle atrophy.* ***C)*** *Myofibers CSA analysis indicates a significant reduction in area of Drp1-null muscles (n=5 mice each group).* ***D)*** *Representative haematoxilin-eosin staining of Tibialis Anterior muscle showing no sign of inflammation or degeneration after Drp1 deletion.* ***E, F)*** *In vivo force measurement analysis demonstrates a decrease in both absolute and normalized forces in knock-out mice (n=3 mice). * p≤0.05; ** p≤0.01.*

3.8 Drp1 deletion leads to alteration in mitochondrial morphology and function

Drp1 is known to play a critical role in the control of mitochondria quality in post mitotic tissues. So, we decided to investigate mitochondria morphology and function after the acute deletion of this fission protein. SDH staining appeared normal, but the increased size of blue puncta in oxidative fibers suggested the presence of bigger mitochondria in Drp1-KO muscles (Fig. 8A). Analysis of mitochondria ultrastructure through electron microscopy confirmed the presence of bigger mitochondria in tamoxifen treated $Drp1^{-/-}$ muscles (Fig. 8B). Since an alteration in mitochondria size and morphology is associated with impaired functionality, we decided to evaluate the capability to maintain mitochondria membrane potential. We performed TMRM assay on FDB single fibers from tamoxifen treated mice. After the addition of oligomycin, an inhibitor of F_1F_0-ATPase (Grumati et al., 2010), $Drp1^{-/-}$ fibers showed a significant increased incidence of mitochondria that depolarized, while control mitochondria maintained membrane potential (Fig. 8C). In addition, TMRM staining revealed some areas of the myofiber where mitochondria were completely depolarized (Fig. 8D).

We therefore evaluated respiratory control ratio (RCR), an index of mitochondria respiration efficiency. Both Complex-I supported (Glutamate/Malate) and Complex-II dependent (Succinate/Rotenone) respiration resulted affected by Drp1 deletion (Fig. 8E). Moreover, also Complex-IV driven (Ascorbate/TMPD) respiration is severely impaired in $Drp1^{-/-}$ mitochondria (Fig. 8F). In conclusion, the absence of Drp1 in adult animals alters mitochondrial morphology and function.

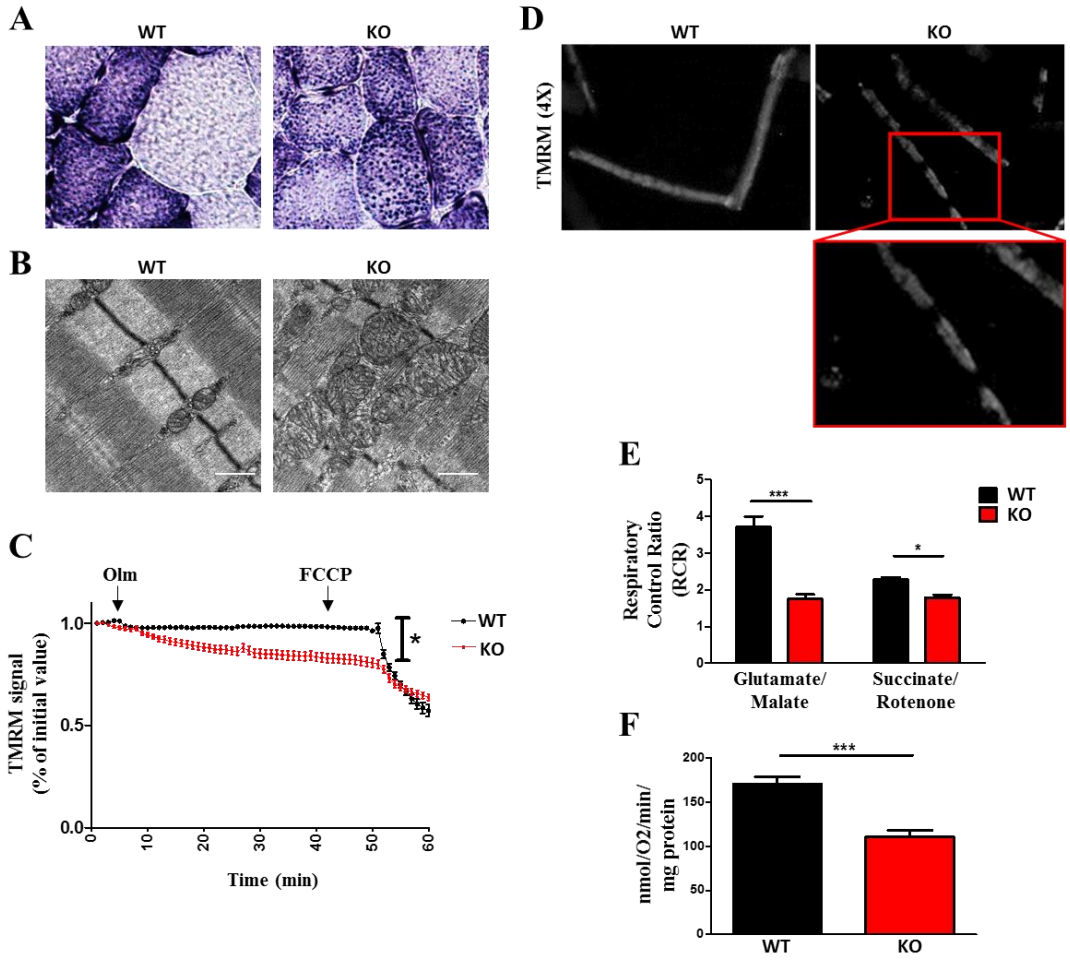

Figure 8: Ablation of Drp1 in adulthood modifies mitochondrial size and RCR. ***A)*** *SDH staining indicating the presence of bigger mitochondria compared to control.* ***B)*** *Drp1 acute deletion leads to defects in mitochondrial shape. Representative electron micrographs of EDL muscles of controls and Drp1$^{-/-}$ confirm the presence of bigger mitochondria in KO animals.* ***C, D)*** *TMRM assay demonstrates that absence of Drp1 induces mitochondrial depolarization (WT, n=15 fibers; KO, n=52 fibers). Mitochondria respiration experiments show an impairment in Complex I-, Complex II- and Complex IV-dependent respiration (**E**, **F**; data represent average of 4 independent experiments). * p≤0.05; *** p≤0.001.*

Mitochondrial respiration depends on the morphology of mitochondria and in particular of cristae, where respiratory chain complexes mainly localize (Vogel et al., 2006). RCC then assembly in quaternary structure named RCS. Mitochondria shape regulate RCS assembly and stability, impacting on respiratory efficiency (Cogliati et al., 2013). We noticed that supercomplexes assembly was impaired in Drp1 deficient mice (Fig. 9A), despite that mitochondrial DNA content and mitochondrial mass revealed by TOM20 and PORIN did not differ between the two genotypes (Fig. 9B, C). In conclusion, Drp1 ablation in adult animals alters mitochondrial morphology and function without changing in mtDNA content.

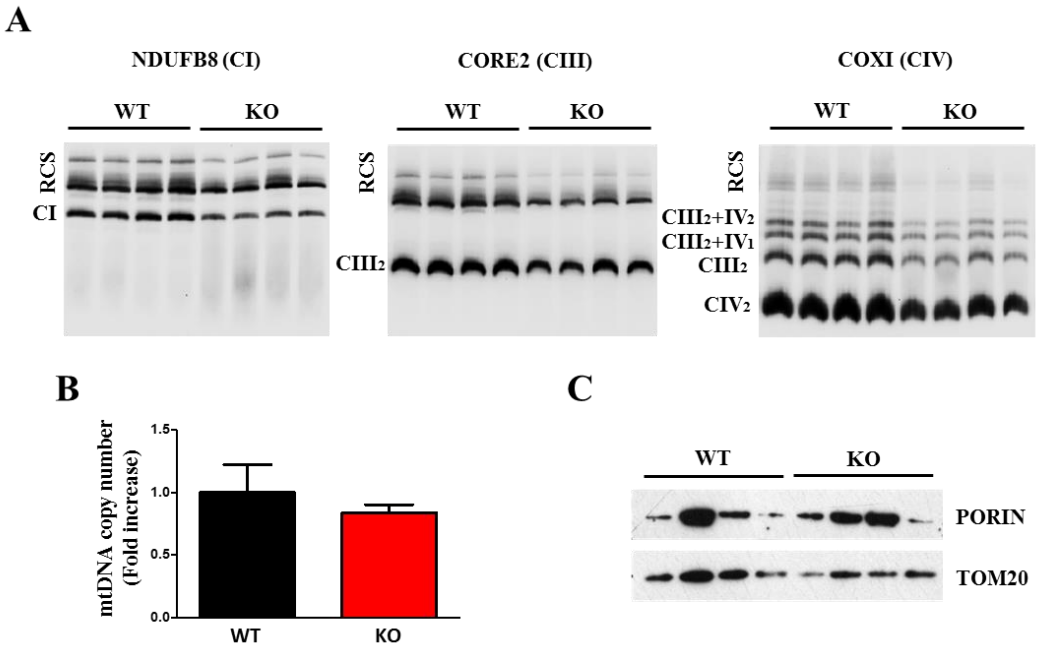

Figure 9: Drp1 deletion impairs RCS assembly. A) *The assembly of CIII and CIV in RCS is significantly reduced in mitochondria of KO muscles. Representative Blue Native PAGE analysis showing RCS developed and normalized for individual respiratory chain complexes. CI subunit NDUFB8 (left panel), CIII-Core2 protein 2 (middle panel) and CIV subunit COXI (right panel). n=5 mice each condition.* ***B)*** *Mitochondrial DNA copy number quantification in controls and KO muscles. mtDNA was amplified by RT-PCR from total DNA of gastrocnemius muscles of the indicated genotype. Data are normalized to controls and represent the average ± SEM of five independent experiments.* ***C)*** *Mitochondrial mass revealed by TOM20 and porin was not affected by Drp1 deletion (n=4 mice).*

3.9 Protein degradation pathways are activated after the ablation of Drp1 in adult muscles

In order to understand the mechanism involved in muscle atrophy, we analyzed both protein synthesis and protein degradation systems after the acute deletion of Drp1. We first, monitored *in vivo* protein synthesis through SUnSET technique, but we did not find any differences between wildtype and knock-out muscles (Fig. 10A).

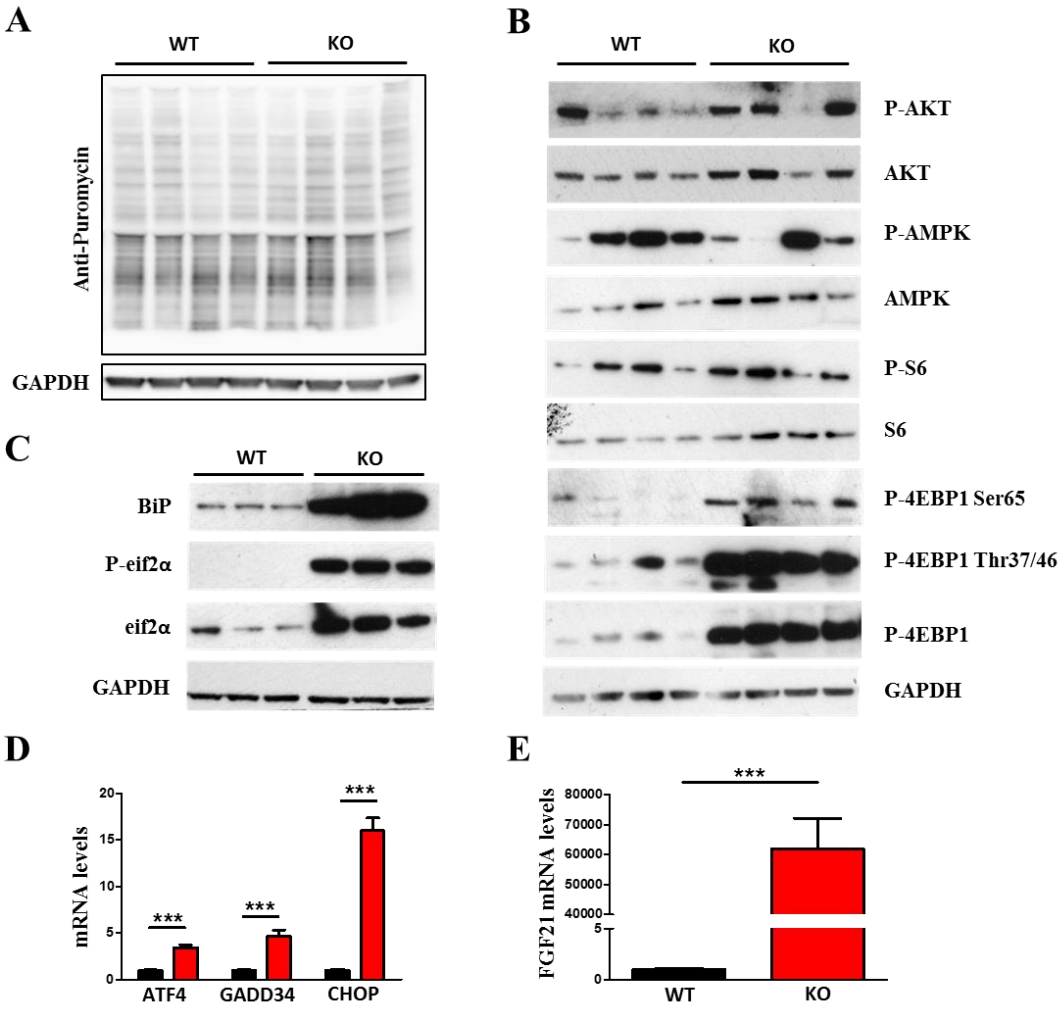

Figure 10: Drp1 acute deletion does not impair protein synthesis despite an increase in UPR. ***A)*** *Total protein extracts from adult muscles treated with puromycin were immunoblotted with reported antibodies (n=4 mice each condition).* ***B)*** *Western Blot analysis show no differences in Akt-mTOR pathway (n=4 mice each condition).*

*Immunoblot **(C)** and RT-PCR **(D)** analysis demonstrating the activation of the UPR pathway in Drp1-null mice (n=6 mice). **E)** FGF21 is highly expressed in KO muscles (n=6 mice). *** p≤0.001.*

Moreover, similarly to the results obtained in conditional Drp1 deficient mice, the Akt-mTOR axis was not affected with the exception of a huge 4EBP1 induction that however was hyper-phosphorylated (Fig. 10B). However, when we moved to check the Unfolded Protein Response pathway, we found a significant increase of Grp78/BiP protein levels and of the hyper-phosphorylated form of eif2α, meaning that UPR is strongly activated in Drp1-depleted muscles (Fig. 10C). In addition, RT-PCR analysis showed an upregulation of ATF4 and its downstream target genes including the cytokine FGF21 (Fig. 10D, E).

Next we monitored protein breakdown focusing on the ubiquitin-proteasome system. Interestingly, the E3 ubiquitin ligases Atrogin1 and Murf1 did not change in $Drp1^{-/-}$ mice, while MUSA1 and Itch were significantly upregulated (Fig. 11A). However, the mild induction of these atrogenes is not sufficient to explain the important reduction of muscle mass. So, we monitored the autophagy-lysosome system and found that the expression levels of most of the autophagy-related genes were induced in the absence of Drp1 (Fig. 11B). In addition, Western Blot analysis revealed a strong accumulation of the autophagy-substrate p62 and of the non-lipidated form of LC3 (LC3 I) in knock-out mice (Fig. 11C). These data suggested that the deletion of Drp1 could result in an impairment of the autophagic flux. In 2014 it was reported that the absence of Drp1 in cardiomyocytes led to an increase in mitochondria connectivity and size, resulting in mitophagy defect (Kageyama et al., 2014; Song et al., 2015). To check if this was happening in our model, we treated control and KO mice with colchicine, a drug that inhibits the autophagosome delivery to the lysosome leading to an accumulation of autophagosomes. After colchicine treatment p62 accumulates more in wildtype than in $Drp1^{-/-}$ treated mice. The same occurred for LC3 II levels (Fig. 11D).

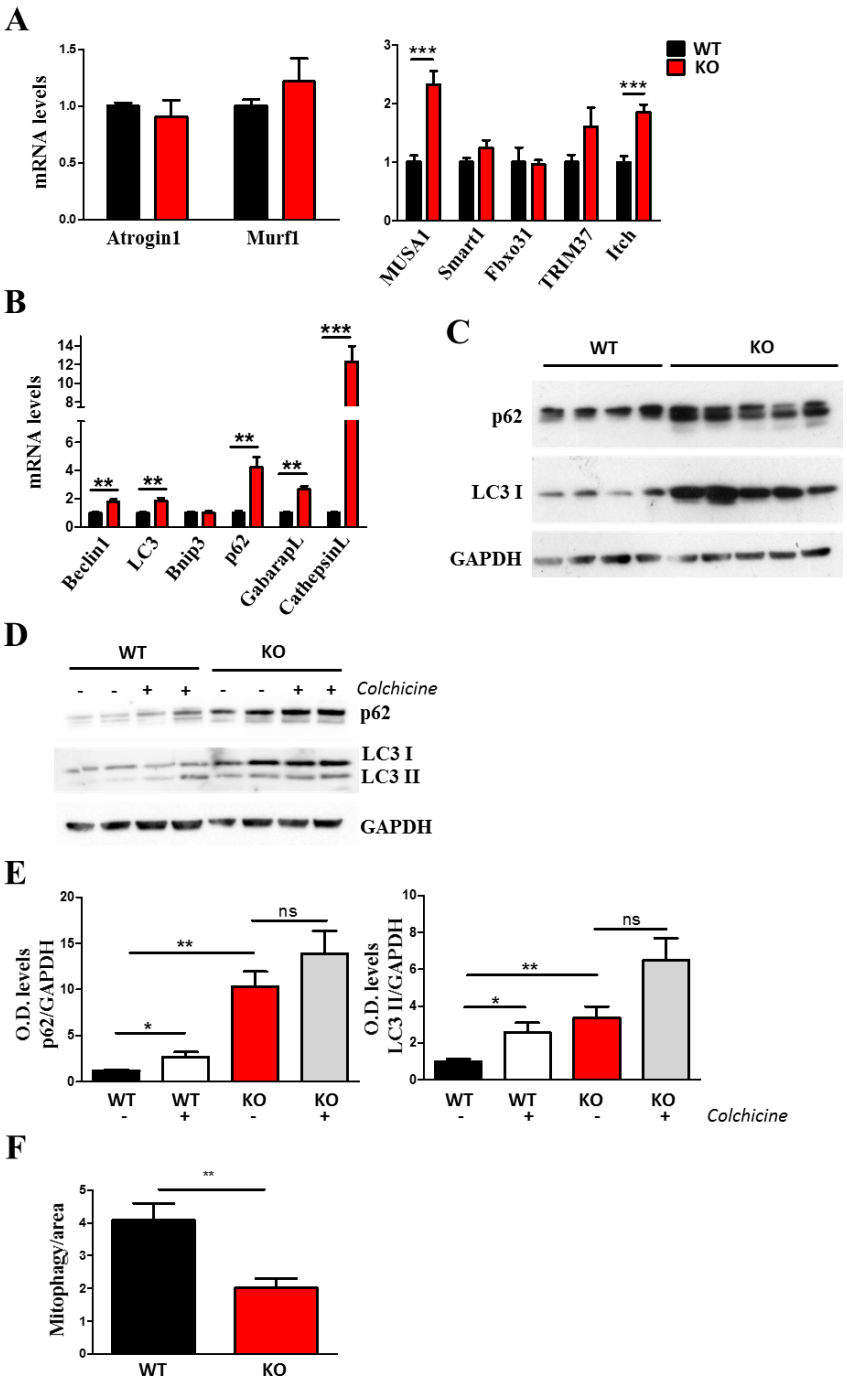

Figure 11: Protein degradation pathways are activated with acute inhibition of Drp1 in adult muscles. ***A)*** *RT-PCR analysis of transcriptional levels of the muscle-specific ubiquitin ligases Atrogin1 and MuRF1 and E3-ligases MUSA1, Smart1, FbxO31, TRIM37 and Itch. (n=6 mice each condition). Real-time PCR* ***(B)*** *and Western Blot* ***(C)*** *analysis of autophagy marker showing an impaired autophagy in Drp1$^{-/-}$ (n=6 mice).* ***D)*** *Immunoblot and relative O.D. levels* ***(E)*** *from colchicine treated mice suggesting a block in autophagic*

flux after Drp1 inhibition (n=5 mice each condition). ***F)*** *Keima Assay demonstrating decreased mitophagy in Drp1-KO myofibers (WT, n=42; KO, n=40). * p≤0.05; ** p≤0.01; *** p≤.0.001.*

In addition, we monitored mitophagy through mt-Keima, a novel fluorescence-based assay that specifically measures autolysosome formation (Katayama et al., 2011). The results obtained indicated that the deletion of Drp1 blocked mitophagy (Fig. 11F). The cause of the impairment of this process is not clear. One possibility is that the increased dimension of mitochondria prevents the engulfment of giant mitochondria into the autophagosome during the initial step of the autophagic flux, leading, therefore, to the accumulation of damaged mitochondria in Drp1 knock-out myofibers.

3.10 Drp1 ablation in adult muscles alters calcium homeostasis

Chronic deletion of Drp1 impaired muscle force, mitochondria functionality and triggered ER stress. In order to connect these different features, we investigated calcium homeostasis. We determined cytosolic free [Ca^{2+}] in FDB isolated fibers with the fluorescent indicator Fura-2 AM. At rest, cytosolic free Ca^{2+} was not significantly different between control and KO mice (Fig. 12A). Interestingly Drp1-null fibers showed a reduction in calcium transients caused by repetitive electrical stimulations, which induced SR-calcium release (Fig. 12B). So, we evaluated intra-SR Ca^{2+} concentration through D1ER Cameleon probe, but we didn't find any changes in KO animals (Fig. 12C). Then we monitored the reduction in SR free [Ca^{2+}] during the train of stimuli, and quantified it by the drop in the ratio at the end of the stimuli. No significant differences were detected in absence of Drp1 (Fig. 12D). An important technical limit is that mitochondria-targeted Cameleon probe is pH-sensitive. pH in Drp1 knock-out mitochondria is lower compared to controls (data not shown). For this reason, we could not analyse directly mitochondria calcium content.

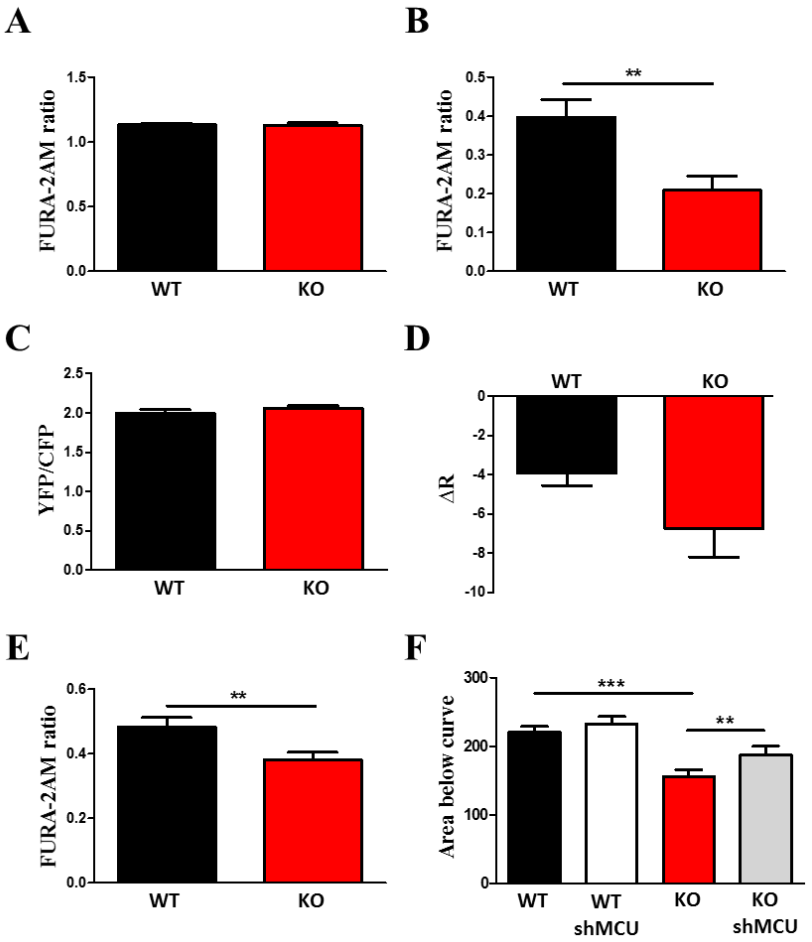

Figure 12: Calcium homeostasis is impaired after the deletion of Drp1. A) *Cytosolic calcium level at rest is not affected in KO muscle. n=19 fibers each condition.* ***B)*** *Cytosolic Ca^{2+} transients induced by electrical pulses is lower in Drp1-null mice. n=19 fibers each.* ***C, D)*** *Intra SR- Ca^{2+} concentration is not affected, neither is the decrease in SR Ca^{2+} levels at the end of electrical stimuli. (C, n=28 fibers each condition, D, n=10 fibers each).* ***E)*** *Calcium transients after stimuli are affected before muscle mass loss. n=25 fibers each.* ***F)*** *Inhibition of mitochondria Ca^{2+} uptake restored cytosolic Ca^{2+} levels during caffeine-thapsigargin treatment. (WT n=17 fibers; WT shMCU n= 23 fibers; KO n=27 fibers; KO shMCU n=17 fibers). **p≤0.01; ***p≤0.001.*

To better understand if the impairment in calcium physiology is an early event that precedes muscle loss, we analysed animals just before they start to loose body weight. Also at this time-point, cytosolic free Ca^{2+} transients after electrical stimulation were lower in knock-out fibers (Fig. 12E). When we treated fibers with

caffeine, a drug that induce Ca^{2+}-release from RyR, and thapsigargin, an inhibitor of SERCA, to induce SR Ca^{2+} emptying, we confirmed the reduction in SR-calcium release in KO muscles (Fig. 12F). Given the incongruence between SR free [Ca^{2+}] and the decrease in SR-calcium release, we checked the role of mitochondria as Ca^{2+} buffers. So, we downregulated MCU through shRNA approach (shMCU) in control and Drp1 null mice and evaluated cytosolic Ca^{2+} levels during caffeine and thapsigargin treatment, after MCU silencing. Surprisingly, the inhibition of mitochondrial Ca^{2+} uptake in knock-out fibers recovered Ca^{2+} released from SR to physiological levels (Fig. 12F). These data indicates that the defect in calcium homeostasis is probably due to mitochondrial calcium overload.

3.11 Chronic deletion of Drp1 triggers severe muscle atrophy

Finally, we wondered about the effects of Drp1 chronic ablation. We monitored mice after 7 months from the deletion of Drp1 and found that knock-out mice appeared smaller compared to controls (Fig. 13A). Moreover $Drp1^{-/-}$ had kyphosis, a typical feature of precocious ageing (Fig. 13B). In addition, both Tibialis Anterior and gastrocnemius muscles appeared extremely atrophic (Fig. 13C). When we analysed muscle morphology, we noticed that about 25% of knock-out myofibers were centrally nucleated, meaning that the chronic deletion of Drp1 triggered fiber degeneration and regeneration (Fig. 13D, E).

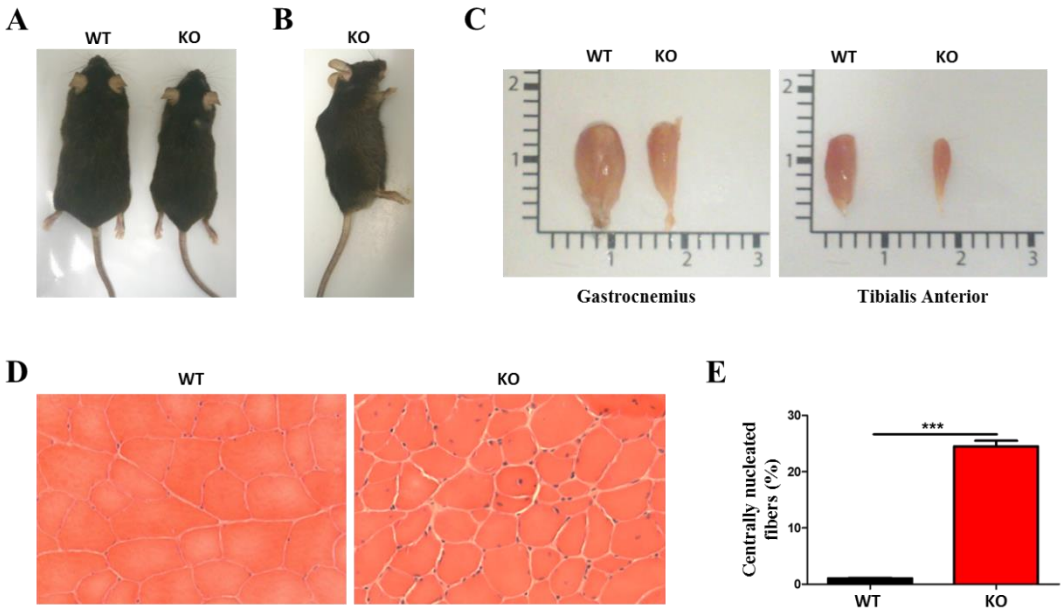

Figure 13: Chronic deletion of Drp1 results in severe muscle atrophy and aging. *Long-term Drp1 deletion triggers signs of precocious aging (**A, B**). **C)** Representative pictures showing huge muscle atrophy 7 months after Drp1 ablation. In Drp1$^{-/-}$ muscles 25% of myofibers are centrally nucleated (**D, E**; n=3 mice each condition). *** p≤0.001.*

4 DISCUSSION

The importance of mitochondrial fusion and fission was underlined by embryonic lethality of mouse knockouts for Opa1, Mfn1 and Mfn2 (Chen et al., 2003; Davies et al., 2007). Moreover, the specific deletion of fusion proteins in skeletal muscle resulted in mitochondria dysfunction and muscle atrophy (Tezze et al., submitted). However, little is known about the role of the mitochondrial fission protein Drp1 in skeletal muscle. Our studies provide insight into the *in vivo* functions of Drp1 in mammals. The obtained data that two different muscle specific knock-out mice used in this study result in striking phenotypes reveals the critical role of mitochondria fission in muscle homeostasis.

From previous studies we know that overexpression of Drp1 is sufficient to activate an atrophy program via AMPK-FoxO3 axis (Romanello et al., 2010). In addition, the conditional muscle-specific Drp1 overexpression triggers muscle mass loss mediated by mitochondrial unfolded protein response pathway, ATF4 induction and reduction in GH sensitivity (Touvier et al., 2015). However, overexpression studies are often confounded by off target effects of the overexpressed gene. In our loss of function study, the conditional Drp1 ablation results in newborns lethality and muscle wasting that is mediated by different pathways including UPR and FGF21 induction. The observed FGF21 induction in muscle results in metabolic changes such as hypoglycemia, GH resistance and decreased IGF1 expression in the liver, and a consequent reduced animal size. These data confirm the importance of muscle as a source of blood FGF21 in presence of mitochondria dysfunction. However, the inhibition of protein synthesis is independent of FGF21 and it is related to signaling pathways that are upstream of FGF21 induction. Indeed, protein synthesis impairment is mainly due to UPR that blocks general translation through eif2α phosphorylation. Nevertheless, the induction of protein breakdown and atrophy-related genes is not related to UPR, in fact atrophy-related genes are not direct target of ATF4 (Ebert et al., 2012; Ebert et al., 2010). Moreover, when we

downregulated ATF4 in our model *in vivo*, knock-out animals were not protected from muscle mass loss (not shown).

FoxO family members have been shown to regulate the two major systems involved in protein breakdown (Milan et al., 2015). In particular, FoxO3 is the main regulator of Atrogin1 (Sandri et al., 2004), and the finding of Atrogin1, MuRF1 and MUSA1 induction in conditional Drp1$^{-/-}$ animals suggests an activation of FoxOs family. While the phosphorylation of Akt, the major upstream regulator of FoxO family, is not affected by Drp1 deletion, it is possible that other kinases or different post-translational modifications are responsible for FoxO activation. It is unlikely that oxidative stress is the trigger of FoxO since we did not reveal an increase of protein carbonylation in Drp1 knock-out mice (not shown). However, it is worth mentioning that mild oxidative stress might be sufficient to activate FoxO.

Drp1 ablation in heart and brain is lethal (Ishihara et al., 2009; Wakabayashi et al., 2009; Kageyama et al., 2014; Ikeda et al., 2015; Song et al., 2015), suggesting the importance of mitochondria fission in post-mitotic tissues. Our study highlights the importance of mitochondrial fission machinery in adult skeletal muscle, indicating that mitochondrial dynamics shall be kept in check not only during development, but also in postnatal life. Indeed a recent study identified that during sarcopenia, the age-related muscle mass loss, muscles are characterized by the progressive loss of mitochondrial proteins involved in fusion and fission processes (Ibedunjo et al., 2013). In addition, different genetic evidences are suggesting that fusion is essential in skeletal and cardiac muscle, impinging on mitochondrial functionality, mtDNA mixing and mitophagy (Chen et al., 2010; Chen et al., 2011; Tezze et al., submitted). However, also Drp1 is required for the maintenance of heart and brain homeostasis through the removal of damaged mitochondria (Ishihara et al., 2009; Wakabayashi et al., 2009; Kageyama et al., 2014; Ikeda et al., 2015; Song et al., 2015). Our studies clarify that also in adult skeletal muscle mitochondrial fission is not dispensable. Both conditional as well as inducible Drp1 deletion lead to similar phenotype, but differences exist in the retrograde signaling from mitochondria to the nucleus upon the two models. However, the activation of the UPR pathway is

conserved between conditional and inducible model. Also the ablation of mitochondrial fusion in muscle leads to UPR activation, at least in *D. melanogaster* (Debattisti et al., 2014). In our model, it is possible that SR, which marks site of mitochondrial division, acts as a sensor of mitochondrial shape and signals it to the nucleus and to the whole organism.

Importantly, the absence of Drp1 impairs muscle force and mitochondria functionality. Moreover, our data suggest that muscle weakness is not dependent on muscle atrophy, but probably is due to a problem in the excitation-contraction coupling in absence of Drp1. We tried to connect these two aspects to UPR by studying calcium homeostasis. Indeed, dysregulation in Ca^{2+} levels leads to ER stress, mitochondria dysfunction and reduced muscle performance through excitation-contraction problems. The importance of mitochondrial calcium uptake in skeletal muscle was recently highlighted by *in vivo* MCU silencing and overexpression. Indeed, Mammucari et al. found that mitochondrial calcium signaling can modulate skeletal muscle trophism (Mammucari et al., 2015). However, the role of mitochondria dynamics in calcium homeostasis is still unclear. Our findings indicate that mitochondria fission is important for the maintenance of the physiology of calcium signaling at least in skeletal muscle. We hypothesized that the block of mitochondria division leads to the presence of enlarged mitochondria that can accumulate calcium more efficiently thus subtracting Ca^{2+} to muscle contraction.

Finally, we investigated mice after 7 months from the deletion of Drp1. Chronic Drp1 ablation led to the accumulation of centrally nucleated myofibers, suggesting that fibers degeneration and regeneration is going on. Myofibers degeneration can be the result of an excessive mitochondrial Ca^{2+} uptake and to the consequent PTP opening. This resembles dystrophic muscles, where mitochondrial dysfunction is thought to result from Ca^{2+} overload which can lead to PTP opening driving to muscle cell death (Percival et al., 2013). Our future plan is to investigate better this mechanism through the concomitant ablation of Drp1 and MCU in skeletal muscle.

In conclusion, our data indicate that mitochondrial fragmentation is critical for muscle mass maintenance and calcium homeostasis. This is supported by previously findings in our laboratory demonstrating that the inhibition of other mitochondrial quality control pathways, such as mitophagy, is an important component in the pathogenesis of sarcopenia (Carnio et al., 2014). Thus, therapeutic interventions that maintain a healthy mitochondrial network could be important for the inherited and acquired disorders characterized by both muscle wasting and mitochondrial dysfunction.

5 BIBLIOGRAPHY

Andresson D.C., Betzenhauser M.J., Reiken S., Meli A.C., Umanskaya A., Xie W., Shiomi T., Zalk R., Lacampagne A., Marks A.R. (2011). Ryanodine receptor oxidation causes intracellular calcium leak and muscle weakness in aging. *Cell Metab.* 14, 196-207.

Antunes D., Padrão A.I., Maciel E., Santinha D., Olivieira P., Vitorino R., Moreira-Gonçalves D., Colaço B., Pires M.J., Nunes C., Santos L.L., Amado F., Duarte J.A., Domingues M.R., Ferreira R. (2014). Molecular insights into mitochondrial dysfunction in cancer-related muscle wasting. *Biochim Biophys. Acta.* 1841, 896-905.

Barrett K.E., Boitano S., Barman S.M., Brooks H.L. (2010). Chapther 5 – Excitable tissue: muscle, in *"Ganong's review of medical physiology"* twenty-third edition.

Bdolah Y., Segal A., Tanksale P., Karumanchi S.A., Lecker S.H. (2007). Atrophy-related ubiquitin ligases atrogin-1 and MuRF-1 are associated with uterine smooth muscle involution in the postpartum period. *Am J Physiol Regul Integr Comp Physiol.* 292, 971-976.

Bernardi, P. (1999). Mitochondrial transport of cations: channels, exchangers, and permeability transition. *Physiol. Rev.* 79, 1127–1155.

Blaauw B., Mammucari C., Toniolo L., Agatea L., Abraham R., Sandri M., Reggiani C., and Schiaffino S. (2008). Akt activation prevents the force drop induced by eccentric contractions in dystrophin-deficient skeletal muscle. *Hum Mol Genet* 17, 3686-3696.

Blei M.L., Conley K.E., and Kushmerick M.J. (1993). Separate measures of ATP utilization and recovery in human skeletal muscle. *J. Physiol.* 465, 203-222.

Bodine S.C., Latres E., Baumhueter S., Lai V.K., Nunez L., Clarke B.A., Poueymirou W.T., Panaro F.J., Na E., Dharmarajan K., Pan Z.Q., Valenzuela D.M., DeChiara T.M., Stitt T.N., Yancopoulos G.D., Glass D.J. (2001). Identification of ubiquitin ligases required for skeletal muscle atrophy. *Science* 294, 1704-1708.

Bothe G.W., Haspel J.A., Smith C.L., Wiener H.H., Burden S.J. (2000). Selective expression of Cre recombinase in skeletal muscle fibers. *Genesis* 26, 165-166.

Braschi E., Zunino R., and McBride H. (2009). MAPL is a new mitochondrial SUMO E3 ligase that regulates mitochondrial fission. *EMBO Rep*. 10, 748-754.

Campello S., Scorrano L. (2010). Mitochondrial shape changes: orchestrating cell pathophysiology. *EMBO Rep*. 11, 678-684.

Canato M., Scorzeto M., Giacomello M., Protasi F., Reggiani C., Stienen G.J. (2010). Massive alterations of sarcoplasmic reticulum free calcium in skeletal muscle fibers lacking calsequestrin revealed by a genetically encoded probe. *Proc Natl Acad Sci USA*. 107, 22326-22331.

Cárdenas C., Miller R.A., Smith I., Bui T., Molgó J., Müller M., Vais H., Cheung K.H., Yang J., Parker I., Thompson C.B., Birnbaum M.J., Hallows K.R., Foskett J.K. (2010). Essential regulation of cell bioenergetics by constitutive InsP3 receptor Ca2+ transfer to mitochondria. *Cell* 142, 270-283.

Carnio S., LoVerso F., Baraibar M.A., Longa E., Khan M.M., Maffei M., Reischl M., Canepari M., Loefler S., Kern H., Blaauw B., Friguet B., Bottinelli R., Rudolf R., Sandri M. (2014). Autophagy impairment in muscles induces neuromuscular junction degeneration and precocious aging. *Cell Rep.* 8, 1509-1521.

Chen H., Detmer S.A., Ewald A.J., Griffin E.E., Fraser E.S., and Chan D.C. (2003). Mitofusins Mfn1 and Mfn2 coordinately regulate mitochondrial fusion and are essential for embryonic development. *J. Cell Biol*. 160, 189-200.

Chen H., Vermulst M., Wang Y., Chomyn A., Prolla T.A., McCaffery J.M., Chan D.C. (2010). Mitochondria fusion is required for mtDNA stability in skeletal muscle and tolerance of mtDNA mutations. *Cell* 141, 280-289.

Chen Y., Liu Y., and Dorn G.W.II. (2011). Mitochondrial fusion is essential for organelle function and cardiac homeostasis. *Circ. Res.* 109, 1327-1331.

Ciciliot S., Rossi A.C., Dyar K.A., Blaauw B., Schiaffino S. (2013). Muscle type and fiber type specificity in muscle wasting. *Int. J. Biochem. Cell Biol.* 45, 2191-2199.

Civiletto G., Varanita T., Cerutti R., Gorletta T., Barbaro S., Marchet S., Lamperti C., Viscomi C., Scorrano L., Zeviani M. (2015). Opa1 overexpression ameliorates the phenotype of two mitochondrial disease mouse models. *Cell Metab.* 21, 845-854.

Cogliati S., Frezza C., Soriano M.E., Varanita T., Quintana-Carbera R., Corrado M., Cipolat S., Costa V., Casarin A., Gomes L.C., Perales-Clemente E., Salviati L., Fernandez-Silva P., Enriquez J.A., and Scorrano L. (2013). Mitochondrial cristae shape determines respiratory chain supercomplexes assembly and respiratory efficiency. *Cell* 155, 160-171.

Crescenzo R., Bianco F., Mazzoli A., Giacco A., Liverini G., and Iossa S. (2014). Mitochondrial efficiency and insulin resistance. *Front. Physiol*. 5:512.

Cribbs J.T., and Strack S. (2007). Reversible phosphorylation of Drp1 by cyclic AMP-dependent protein kinase and calcineurin regulates mitochondrial fission and cell death. *EMBO Rep*. 8, 939-944.

Davies V.J., Hollins A.J., Piechota M.J., Yip W., Davies J.R., White K.E., Nicols P.P., Boulton M.E., Votruba M. (2007). Opa1 deficiency in a mouse model of autosomal dominant optic atrophy impairs mitochondrial morphology, optic nerve structure and visual function. *Hum. Mol. Genet.* 16, 1307-1318.

de Brito O.M., and Scorrano L. (2009). Mitofusin-2 regulates mitochondrial and endoplasmic reticulum morphology and tethering: the role of Ras. *Mitochondrion* 9, 222-226.

Debattisti V., Pendin D., Ziviani E., Daga A., Scorrano L. (2014). Reduction of endoplasmic reticulum stress attenuates the defects caused by Drosophila mitofusin depletion. *J Cell Biol*. 204, 303-312.

Durham, W.J., Aracena-Parks, P., Long, C., Rossi, A.E., Goonasekera, S.A., Boncompagni, S., Galvan, D.L., Gilman, C.P., Baker, M.R., Shirokova, N., Protasi F., Dirksen R., Hamilton S.L. (2008). RyR1 S-nitrosylation underlies environmental heat stroke and sudden death in Y522S RyR1 knockin mice. *Cell* 133, 53–65.

Ebert S.M., Monteys A.M., Fox D.K., Bongers K.S., Shields B.E., Malmberg S.E., Davidson B.L., Suneja M., Adams C.M. (2010). The transcription factor ATF4 promotes skeletal myofiber atrophy during fasting. *Mol Endocrinol*. 24, 790-799.

Ebert S.M., Dyle M.C., Kunkel S.D., Bullard S.A., Bongers K.S., Fox D.K., Dierdorff J.M., Foster E.D., Adams C.M. (2012). Stress-induced skeletal muscle Gadd45a expression reprograms myonuclei and causes muscle atrophy. *J Biol Chem.* 287, 27290-27301.

Elgass K., Pakay J., Ryan M.T., Palmer C.S. (2013). Recent advances into the understanding of mitochondrial fission. *Biochim Biophys Acta*. 1833, 150-161.

Frezza C., Cipolat S., de Brito M.O., Micaroni M., Beznoussenko G.V., Rudka T., Bartoli D., Polishuck R.S., Danial N.N., De Strooper B., Scorrano L. (2006). OPA1 controls apoptotic cristae remodelling independently from mitochondrial fusion. *Cell.* 126, 177-189.

Frezza C., Cipolat S., Scorrano L. (2007). Organelle isolation: functional mitochondria from mouse liver, muscle and cultured fibroblast. *Nat Protoc.* 2, 287-295.

Gaitanos G.C., Williams C., Boobis L.H., and Brooks S. (1993). Human muscle metabolism during intermittent maximal exercise. *J. Appl. Physiol*. 75, 712-719.

Germain M., Mathai J.P., McBride H.M., Shore G.C. (2005). Endoplasmic reticulum BIK initiates DRP1-regulated remodelling of mitochondrial cristae during apoptosis. *EMBO J.* 24, 1546-1556.

Glass D.J. (2005). Skeletal muscle hypertrophy and atrophy signaling pathways. *Int J Biochem Cell Biol*. 37, 1974-1984.

Gomes M.D., Lecker S.H., Jagoe R.T., Navon A., and Goldberg A.L. (2001). Atrogin-1, a muscle-specific F-box protein highly expressed during muscle atrophy. *Proc. Natl. Acad. Sci. U.S.A.* 98, 1440-1445.

Gomes L.C., Scorrano L. (2013). Mitochondrial morphology in mitophagy and macroautophagy. *Biochim Biophys Acta*. 1833, 205-212.

Goodman C.A., Mabrey D.M., Frey J.W., Miu M.H., Schmidt E.K., Pierre P., Hornberger T.A. (2011). Novel insights into the regulation of skeletal muscle protein synthesis as revealed by a new nonradioactive in vivo technique. *FASEB J.* 25, 1028-1039.

Grumati P., Coletto L., Sabatelli P., Cescon M., Angelin A., Bertaggia E., Blaauw B., Urciuolo A., Tiepolo T., Merlini L., et al. (2010). Autophagy is defective in collagen VI muscular dystrophies, and its reactivation rescues myofiber degeneration. *Nat. Med.* 16, 1313-1320.

Hoppeler H. (1986). Exercise-induced ultrastructural changes in skeletal muscle. *Int. J. Sports Med*. 7, 187-204.

Ibebunjo C., Chick J.M., Kendall T., Eash J.K., Li C., Zhang Y., Vickers C., Wu Z., Clarke B.A., Shi J., Cruz J., Fournier B., Brachat S., Gutzwiller S., Ma Q., Markovits J., Broome M., Steinkrauss M., Skuba E., Galarneau J.R., Gygi S.P., Glass D.J. (2013). Genomic and proteomic profiling reveals reduced

mitochondrial function and disruption of the neuromuscular junction driving rat sarcopenia. *Mol. Cell Biol.* 33, 194-212.

Ichimura Y., Komatsu M. (2010). Selective degradation of p62 by autophagy. *Semin. Immunopathol.* 32, 431-436.

Ikeda Y., Shirakabe A., Maejima Y., Zhai P., Sciaretta S., Toli J., Nomura M., Mihara K., Egashira K., Ohishi M., Abdellatif M., Sadoshima J. (2015). Endgenous Drp1 mediates mitochondrial autophagy and protects the heart against energy stress. *Circ. Res*. 116, 264-278.

Inagaki T., Lin V.Y., Goetz R., Mohammadi M., Mangelsdorf D.J., Kliewer S.A. (2008). Inhibition of growth hormone signaling by the fasting-induced hormone FGF21. *Cell Metab*. 8, 77-83.

Ishihara N., Nomura M., Jofuku A., Kato H., Suzuki S.O., Masuda K., Otera H., Nakanishi Y., Nonaka I., Goto Y., Taguchi N., Morinaga H., Maeda M., Takayanagi R., Yokota S., Mihara K. (2009). Mitochondrial fission factor Drp1 is essential for embryonic development and synapse formation in mice. *Nat. Cell. Biol*. 11, 958-966.

Ju J.S., Varadhachary A.S., Miller S.E., Weihl C.C. (2010). Quantification of "autophagic flux" in mature skeletal muscle. *Autophagy* 6, 929-935.

Kageyama Y., Hoshijima M., Seo K., Bedja D., Sysa-Shah P., Andrabi S.A., Chen W., Höke A., Dawson V.L., Dawson T.M., Gabrielson K., Kass D.A., Iijima M., Sesaki H. (2014). Parkin-dependent mitophagy requires Drp1 and maintains the integrity of mammalian heart and brain. *EMBO J*. 33, 2798-2813.

Kanki T., Wang K., Klionsky D.J. (2010). A genomic screen for yeast mutants defective in mitophagy. *Autophagy* 6, 278-280.

Karren M.A., Coonrod E., Andreson T.K., and Shaw J.M. (2005). The role of Fis1p-Mdv1p interactions in mitochondrial fission complex assembly. *J. Cell. Biol*. 171, 291-301.

Katayama H., Kogure T., Mizushima N., Yoshimori T., Miyawaki A. (2011). A sensitive and quantitative technique for detecting autophagic events based on lysosomal delivery. *Chem. Biol.* 18, 1042-1052.

Katsetos C.D., Koutzaki S., and Melvin J.J. (2013). Mitochondrial dysfunction in neuromuscular disorders. *Semin. Pediatr. Neurol*. 20, 202-215.

Kim K.H., Jeong Y.T., Oh H., Kim S.H., Cho J.M., Kim Y.N., Kim S.S., Kim do H., Hur K.Y., Kim H.K., Ko T., Han J., Kim H.L., Kim J., Back S.H., Komatsu M., Chen H., Chan D.C., Konishi M., Itoh N., Choi C.S., Lee MS. (2013). Autophagy deficiency leads to protection from obesity and insulin resistance by inducing Fgf21 as a mitokine. *Nat Med* 19, 83-92.

Kirichok Y., Krapivinsky G., Clapham D.E. (2004). The mitochondrial calcium uniporter is a highly selective ion channel. *Nature* 427, 360-364.

Lecker S.H., Jagoe R.T., Gilbert A., Gomes M., Baracos V., Bailey J., Price S.R., Mitch W.E., Goldberg A.L. (2004). Multiple types of skeletal muscle atrophy involve a common program of changes in gene expression. *FASEB J.* 18, 39-51.

Lee Y.J., Jeong S.Y., Karbowski M., Smith C.L., and Youle R.J. (2004). Roles of the mammalian mitochondrial fission and fusion mediators Fis1, Drp1, and Opa1 in apoptosis. *Mol. Biol. Cell*. 15, 5001-5011.

Light N., Champion A.E. (1984). Characterization of muscle epimysium, perimysium and endomysium collagen. *Biochem J.* 219, 1017-1026.

Logan C.V., Szabadkai G., Sharpe J.A., Parry D.A., Torelli S., Childs A.M., Kriek M., Phadke R., Johnson C.A., Roberts N.Y., Bonthron D.T., Pysden K.A., Whyte T., Munteanu I., Foley A.R., Wheway G., Szymanska K., Natarajan S., Abdelhamed Z.A., Morgan J.E., Roper H., Santen G.W., Niks E.H., van der Pol W.L., Lindhout D., Raffaello A., De Stefani D., den Dunnen J.T., Sun Y., Ginjaar I., Sewry C.A., Hurles M., Rizzuto R.; UK10K Consortium., Duchen M.R., Muntoni F., Sheridan E. (2014). Loss-of-function mutations in MICU1 cause a

brain and muscle disorder linked to primary alterations in mitochondrial calcium signaling. *Nat. Genet.* 46, 188-193.

Mammucari C., Milan G., Romanello V., Masiero E., Rudolf R., Del Piccolo P., Burden S.J., Di Lisi R., Sandri C., Zhao J., Goldberg A.L., Schiaffino S., Sandri M. (2007). FoxO3 controls autophagy in skeletal muscle in vivo. *Cell Metab*. 6, 458–471.

Mammucari C., Schiaffino S., and Sandri M. (2008). Downstream of Akt: FoxO3 and mTOR in the regulation of autophagy in skeletal muscle. *Autophagy* 4, 524–526.

Mammucari C., Gherardi G., Zamparo I., Raffaello A., Boncompagni S., Chemello F., Cagnin S., Braga A., Zanin S., Pallafacchina G., Zentilin L., Sandri M., De Stefani D., Protasi F., Lanfranchi G., Rizzuto R. (2015). The mitochondrial calcium uniporter controls skeletal muscle trophism in vivo. *Cell Rep*. 10, 1269-1279.

Masiero E., Agatea L., Mammucari C., Blaauw B., Loro E., Komatsu M., Metzger D., Reggiani C., Schiaffino S., and Sandri M. (2009). Autophagy is required to maintain muscle mass. *Cell Metab.* 10, 507-515.

McCormack J.G., Halestrap A.P., Denton R.M. (1990). Role of calcium ions in regulation of mammalian intramitochondrial metabolism. *Physiol. Rev*. 70, 391-425.

Milan G., Romanello V., Pescatore F., Armani A., Paik J.H., Frasson L., Seydel A., Zhao J,. Abraham R., Goldberg A.L., Blaauw B., DePinho R.A., Sandri M. (2015). Regulation of autophagy and the ubiquitin-proteasome system by the FoxO transcriptional network during muscle atrophy. *Nat. Comm.* 6, 6670.

Mizushima N., and Komatsu M. (2011). Autophagy: renovation of cells and tissues. *Cell* 147, 728-741.

Murgia M., Serrano A.L., Calabria E., Pallafacchina G., Lomo T., Schiaffino S. (2000). Ras is involved in nerve-activity-dependent regulation of muscle genes. *Nat. Cell Biol*. 2, 142-147.

Narendra D., Tanaka A., Suen D., and Youle R.J. (2008). Parkin is recruited selectively to impaired mitochondria and promotes their autophagy. *J. Cell Biol*. 183, 795-803.

Ogata T., and Yamasaki Y. (1985). Scanning electron-microscopic studies on the three-dimensional structure of mitochondria in the mammalian red, white and intermediate muscle fibers. *Cell Tissue Res.* 241, 251-256.

Otera H., Ishihara N., and Mihara K. (2013). New insights into the function and regulation of mitochondrial fission. *Biochim. Biophys. Acta* 1833, 1256-1268.

Palmer C.S., Osellame L.D., Laine D., Koutsopoulos O.S., Frazier A.E., and Ryan M.T. (2011). MiD49 and MiD51, new components of the mitochondrial fission machinery. *EMBO Rep*. 12, 565-573.

Pan X., Liu J., Nguyen T., Liu C., Sun J., Teng Y., Fergusson M.M., Rovira I.I., Allen M., Springer D.A., Aponte A.M., Gucek M., Balaban R.S., Murphy E., Finkel T. (2013). The physiological role of mitochondrial calcium revealed by mice lacking the mitochondrial calcium uniporter. *Nat. Cell Biol*. 15, 1464-1472.

Paolini C., Quarta M., Nori A., Boncompagni S., Canato M., Volpe P., Allen P.D., Reggiani C., Protasi F. (2007). Reorganized stores and impaired calcium handling in skeletal muscle of mice lacking calsequestrin-1. *J. Physiol*. 583, 767-784.

Percival J.M., Siegel M.P., Knowels G., Marcinek D.J. (2013). Defects in mitochondrial localization and ATP synthesis in the mdx mouse model of Duchenne muscular dystrophy are not alleviated by PDE5 inhibition. *Hum. Mol. Genet*. 22, 153-167.

Pette D., Heilmann C. (1979). Some characteristics of sarcoplasmic reticulum in fast- and slow-twitch muscles. *Biochem Soc Trans*. 7, 765-767.

Pfaffl M.W., Lange I.G., Daxenberger A., Meyer H.H. (2001). Tissue-specific expression pattern of estrogen receptors (ER): quantification of ER alpha and ER beta mRNA with real-time RT-PCR. *APMIS*. 109, 345-355.

Proikas-Cezanne T., Codogno P. (2011). A new fluorescence-based assay for autophagy. *Chem Biol.* 18, 940-941.

Raben N., Hill V., Shea L., Takikita S., Baum R., Mizushima N., Ralston E., Plotz P. (2008). Suppression of autophagy in skeletal muscle uncovers the accumulation of ubiquitinated proteins and their potential role in muscle damage in Pompe disease. *Hum. Mol. Genet*. 17, 3897-3908.

Rizzuto R., Pinton P., Carrington W., Fay F.S., Fogarty K.E., Lifshitz L.M., Tuft R.A., Pozzan T. (1998). Close contacts with the endoplasmic reticulum as determinants of mitochondrial Ca^{2+} responses. *Science* 280, 1763-1766.

Rizzuto R., De Stefani D., Raffaello A., Mammucari C. (2012). Mitochondria as sensor and regulators of calcium signalling. *Nat. Rev. Mol*. 13, 566-578.

Romanello V., Guadagnin E., Gomes L., Roder I., Sandri C., Petersen Y., Milan G., Masiero E., Del Piccolo P., Foretz M., Scorrano L., Rudolf R., Sandri M. (2010). Mitochondrial fission and remodelling contributes to muscle atrophy. *EMBO J.* 29, 1774-1785.

Romanello V., and Sandri M. (2016). Mitochondrial quality control and muscle mass maintenance. *Front Physiol.* 6, 422.

Rossi A.E., Boncompagni S., and Dirksen R.T. (2009). Sarcoplasmic reticulum-mitochondrial symbiosis: bidirectional signaling in skeletal muscle. *Exerc. Sport Sci Rev*. 27, 29-35.

Rubinsztein D.C., Marino G., and Kroemer G. (2011). Autophagy and aging. *Cell* 146, 682-695.

Sacheck J.M., Hyatt J.P., Raffaello A., Jagoe R.T., Roy R.R., Edgerton V.R., Lecker S.H., Goldberg A.L. (2007). Rapid disuse and denervation atrophy involve transcriptional changes similar to those of muscle wasting during systemic diseases. *FASEB J*. 21, 140-155.

Sandri M., Sandri C., Gilbert A., Skurk C., Calabria E., Picard A., Walsh K., Schiaffino S., Lecker S.H., Goldberg A.L. (2004). Foxo transcription factors induce the atrophy-related ubiquitin ligase atrogin-1 and cause skeletal muscle atrophy. *Cell* 117, 399-412.

Sandri M. (2013). Protein breakdown in muscle wasting: role of autophagy-lysosome and ubiquitin-proteasome. *Int. J. Biochem. Cell Biol*. 45, 2121-2129.

Sandri M., Coletto L., Grumati P, and Bonaldo P. (2013). Misregulation of autophagy and proten degradation systems in myopathies and muscular dystrophies. *J. Cell Sci.* 126, 5325-5333.

Santel A., Fuller M.T. (2001). Control of mitochondrial morphology by a human mitofusin. *J. Cell Sci.* 114, 867-874.

Santo-Domingo J., Demaurex N. (2010). Calcium uptake mechanisms of mitochondria. *Biochim Biophys. Acta* 1797, 907-912.

Sartori R., Schirwis E., Blaauw B., Bortolanza S., Zhao J., Enzo E., Stantzou A., Mouisel E., Toniolo L., Ferry A., Stricker S., Goldberg A.L., Dupont S., Piccolo S., Amthor H., Sandri M. (2013). BMP signaling controls muscle mass. *Nat Genet.* 45, 1309-1318.

Scherz-Shouval R., Weidberg H., Gonen C., Wilder S., Elazar Z., Oren M. (2010). p53-dependent regulation of autophagy protein LC3 supports cancer cell survival under prolonged starvation. Proc *Natl Acad Sci U S A.* 107, 18511-18516.

Schiaffino S., Reggiani C. (1996). Molecular diversity of myofibrillar proteins: gene regulation and functional significance. *Physiol Rev*. 76, 371-423.

Schiaffino S., Reggiani C. (2011). Fiber types in mammalian skeletal muscles. *Physiol Rev.* 91, 1447-1531.

Schiaffino S., Sandri M., Murgia M. (2007). Activity-dependent signaling pathways controlling muscle diversity and plasticity. *Physiology (Bethesda).* 22, 269-278.

Schiaffino S., Dyar K.A., Ciciliot S., Blaauw B., Sandri M. (2013). Mechanisms regulating skeletal muscle growth and atrophy. *FEBS J. 280*, 4294-4314.

Schmidt E.K., Clavarino G., Ceppi M., Pierre P. (2009). SUnSET, a nonradioactive method to monitor protein synthesis. *Nat Methods*. 6, 275-277.

Schneider M.F. (1994). Control of calcium release in functioning skeletal muscle fibers. *Annu. Rev. Physiol*. 56, 463-484.

Schuler M., Ali F., Metzger E., Chambon P., Metzger D. (2005). Temporally controlled targeted somatic mutagenesis in skeletal muscles of the mouse. *Genesis.* 41, 165-170.

Scorrano L. (2013). Keeping mitochondria in shape: a matter of life and death. *Eur J Clin Invest* 43, 886-893.

Smirnova E., Shurland D.L., Ryazantsev S.N., and van der Bliek M.A. (1998). A Human Dynamin-related Protein Controls the Distribution of Mitochondria. *J. Cell Biol*. 143, 351–358.

Smirnova E., Griparic L., Shurland D.L., and van der Bliek M.A. (2001). Dynamin-related Protein Drp1 Is Required for Mitochondrial Division in Mammalian Cells. *Mol. Biol. Cell* 12, 2245-2256.

Song M., Mihara K., Chen Y., Scorrano L., and Dorn G.W.II. (2015). Mitochondrial fission and fusion factors reciprocally orchestrate mitophagic culling in mouse heart and cultured fibroblasts. *Cell Metab.* 21, 273-285.

Sun N., Yun J., Liu J., Malide D., Liu C., Rovira I.I., Holmström K.M., Fergusson M.M., Yoo Y.H., Combs C.A., Finkel T. (2015). Measuring In Vivo Mitophagy. *Mol. Cell* 60, 685-696.

Suomalainen A., Elo J.M., Pietiläinen K.H., Hakonen A.H., Sevastianova K., Korpela M., Isohanni P., Marjavaara S.K., Tyni T., Kiuru-Enari S., Pihko H., Darin N., Õunap K., Kluijtmans L.A., Paetau A., Buzkova J., Bindoff L.A., Annunen-Rasila J., Uusimaa J., Rissanen A., Yki-Järvinen H., Hirano M., Tulinius M., Smeitink J., Tyynismaa H. (2011). FGF-21 as a biomarker for muscle-manifesting mitochondrial respiratory chain deficiencies: a diagnostic study. *Lancet. Neurol.* 10, 806-818.

Taguchi N., Ishihara N., Jofuku A., Oka T., Mihara K. (2007). Mitotic phosphorylation of dynamin-related GTPase Drp1 participates in mitochondrial fission. *J. Biol. Chem.* 282, 11521-11529.

Tan C.C., Yu J.T., Tan M.S., Jiang T., Zhu X.C., Tan L. (2013). Autophagy in aging and neurodegenerative diseases: implications for pathogenesis and therapy. *Ageing Res Rev*. 12, 237-252.

Touvier T., De Palma C., Rigamonti E., Scagliola A., Incerti E., Mazelin L., Thomas J.L., D'Antonio M., Politi L., Schaeffer L., Clementi E., Brunelli S. (2015). Muscle-specific Drp1 overexpression impairs skeletal muscle growth via translational attenuation. *Cell Death Dis.* 6:e1663.

Twig G., Elorza A., Molina A.J., Mohamed H., Wikstrom J.D., Walzer G., Stiles L., Haigh S.E., Katz S., Las G., Alroy J., Wu M., Py B.F., Yuan J., Deeney J.T., Corkey B.E., Shirihai O.S. (2008). Fission and selective fusion govern mitochondrial segregation and elimination by autophagy. *EMBO J.* 27, 433-446.

Tyynismaa H., Carroll C.J., Raimundo N., Ahola-Erkkilä S., Wenz T., Ruhanen H., Guse K., Hemminki A., Peltola-Mjøsund K.E., Tulkki V., Oresic M., Moraes C.T., Pietiläinen K., Hovatta I., Suomalainen A. (2010). Mitochondrial myopathy induces a starvation-like response. *Hum Mol Genet.* 20, 3948-3958.

Vandanmagsar B., Warfel J.D., Wicks S.E., Ghosh S., Salbaum J.M., Burk D., Dubuisson O.S., Mendoza T.M., Zhang J., Noland R.C., Mynatt R.L. (2016). Impaired Mitochondrial Fat Oxidation Induces FGF21 in Muscle. *Cell Rep*. 15, 1686-1699.

Varanita T., Soriano M.E., Romanello V., Zaglia T., Quintana-Cabrera R., Semenzato M., Menabò R., Costa V., Civiletto G., Pesce P., Viscomi C., Zeviani M., Di Lisa F., Mongillo M., Sandri M., Scorrano L. (2015). The OPA1-dependent mitochondrial cristae remodeling pathway controls atrophic, apoptotic, and ischemic tissue damage. *Cell Metab.* 21, 8348-44.

Vogel F., Bornhövd C., Neupert W., Reichert A.S. (2006). Dynamic subcompartmentalization of the mitochondrial inner membrane. *J Cell Biol*. 175, 237-247.

Wakabayashi J., Zhang Z., Wakabayashi N., Tamura Y., Fukaya M., Kensler T.W., Iijima M., Sesaki H. (2009). The dynamin-related GTPase Drp1 is required for embryonic and brain development in mice. *J. Cell Biol.* 186, 805-816.

Waterham H.R., Koster J., van Roermund C.W., Mooyer P.A., Wanders R.J., Leonard J.V. (2007). A lethal defect of mitochondrial and peroxisomal fission. *N. Engl. J. Med.* 356, 1736-1741.

Zhao J., Brault J.J., Schild A., Cao P., Sandri M., Schiaffino S., Lecker S.H., and Goldberg A.L. (2007). FoxO3 coordinately activates protein degradation by the autophagic/lysosomal and proteasomal pathways in atrophying muscle cells. *Cell Metab*. 6, 472–483.

Zhao J., Brault J.J., Schild A., and Goldberg A.L. (2008). Coordinate activation of autophagy and the proteasome pathway by FoxO transcription factor. *Autophagy* 4, 378–380.